HHS Public Access

Author manuscript

Nat Metab. Author manuscript; available in PMC 2022 May 11.

Published in final edited form as:

Nat Metab. 2021 November ; 3(11): 1484–1499. doi:10.1038/s42255-021-00480-x.

Fibroblast pyruvate carboxylase is required for collagen production in the tumor microenvironment

Simon Schwörer[1], **Natalya N. Pavlova**[1,†], **Francesco V. Cimino**[1,†], **Bryan King**[1], **Xin Cai**[1], **Gina M. Sizemore**[2,3], **Craig B. Thompson**[1,*]

[1]Cancer Biology and Genetics Program, Sloan Kettering Institute, Memorial Sloan Kettering Cancer Center, New York, NY

[2]The Comprehensive Cancer Center, The Ohio State University, Columbus, OH

[3]Department of Radiation Oncology, The Ohio State University, Columbus, OH

Abstract

The aberrant production of collagen by fibroblasts is a hallmark of many solid tumors and can influence cancer progression. How the mesenchymal cells in the tumor microenvironment maintain their production of extracellular matrix proteins as the vascular delivery of glutamine and glucose becomes compromised remains unclear. Here we show that pyruvate carboxylase (PC)-mediated anaplerosis in tumor-associated fibroblasts contributes to tumor fibrosis and growth. Using cultured mesenchymal and cancer cells, as well as mouse allograft models, we provide evidence that extracellular lactate can be utilized by fibroblasts to maintain TCA cycle anaplerosis and non-essential amino acid biosynthesis through PC activity. Furthermore, we show that fibroblast PC is required for collagen production in the tumor microenvironment. These results establish TCA cycle anaplerosis as a determinant of extracellular matrix collagen production, and identify PC as potential target to inhibit tumor desmoplasia.

Introduction

Fibroblasts are mesenchymal cells that play an integral part in the wound healing response. Following disruption of tissue homeostasis, resting fibroblasts are recruited to the site of

*Correspondence to: Craig B. Thompson, Memorial Sloan Kettering Cancer Center, 1275 York Ave., New York, NY 10065, USA, Tel.: (212) 639-6561, Fax: (212) 717-3299, thompsonc@mskcc.org.

†These authors contributed equally to this work

Author Contributions

S.S. conceived the project, performed most experiments, analyzed data, interpreted results, and wrote and edited the manuscript. N.N.P. performed and analyzed tRNA charging experiments. F.V.C. provided technical assistance. B.K. provided support for PSC isolation and characterization and experiments with KPC cells. X.C. provided key knowledge and optimized conditions for experiments with lactate. G.M.S. provided cell lines, interpreted results and edited the manuscript. C.B.T. conceived the project, interpreted results, and wrote and edited the manuscript. All authors participated in discussing and finalizing the manuscript.

Competing interests

C.B.T. is a founder of Agios Pharmaceuticals and a member of its scientific advisory board. He is also a former member of the Board of Directors and stockholder of Merck and Charles River Laboratories. He holds patents related to cellular metabolism. All other authors do not declare any conflict of interest.

injury where they become activated by pro-fibrotic stimuli to upregulate the synthesis and secretion of extracellular matrix (ECM) proteins such as collagen to promote regeneration of the damaged parenchyma [1]. Cancer arises from oncogenic mutations in parenchymal cells, leading to cellular transformation and excessive cell proliferation [2]. This insult to the functional parenchyma disrupts normal tissue homeostasis and initiates a tissue repair response that involves the activation of fibroblasts by growth factors such as TGFβ, resulting in the development of a desmoplastic tumor stroma characterized by excessive deposition of ECM, including collagens [1]. In some tumors such as breast cancer (BRCA) and pancreatic ductal adenocarcinoma (PDAC), the desmoplastic stroma comprises up to 90% of tumor mass [3], and the aberrant presence of ECM proteins or enrichment of an ECM expression signature is associated with poor prognosis across cancer types [4–6]. The ECM modulates virtually all hallmarks of cancer [7]; for example, increased collagen I density promotes mammary tumor initiation, growth and invasion [8]. Thus, targeting ECM synthesis in stromal fibroblasts emerges as potential strategy to limit cancer progression in desmoplastic tumors.

In vitro, the ability of profibrotic stimuli to promote ECM synthesis is supported by metabolic reprogramming [9]. For example, TGFβ promotes the uptake of glucose and glutamine and their utilization for glycine and proline biosynthesis, respectively, to meet the demand for glycine and proline imposed by excessive collagen synthesis [10,11]. In addition, TGFβ increases the mitochondrial oxidation of glucose and glutamine carbon to support the bioenergetic demand of increased translation of ECM proteins [11]. Thus, an abundant supply of these major nutrients as present in standard cell culture media can support a high rate of ECM synthesis. However, glucose and glutamine concentrations in human plasma are lower compared to what is used *in vitro* [12], and their concentrations in the microenvironments of many tumors and certain types of healing wounds are further reduced, due to vascular compromise and/or excess tumor cell nutrient consumption [13]. For example, glutamine levels profoundly drop following tissue injury [14], and glutamine and glucose are among the most depleted nutrients in tumors [15–17].

It remains unclear how the mesenchymal cells in the tumor microenvironment maintain their production of ECM proteins as the vascular delivery of glutamine and glucose becomes compromised. Here, we show that extracellular lactate can be utilized to maintain TCA cycle anaplerosis and non-essential amino acid biosynthesis through the activity of pyruvate carboxylase, and that fibroblast pyruvate carboxylase is required for collagen production in the tumor microenvironment.

Results

TGFβ-induced collagen synthesis is glutamine dependent

To investigate the response of fibroblasts to glutamine limitation, NIH-3T3 cells were cultured in media with glutamine (Gln) concentrations ranging from 2 mM (100%) to 0.2 mM (10%), in the presence or absence of TGFβ. In culture medium containing 100% and 50% Gln, TGFβ stimulation did not change cell proliferation over three days but upregulated collagen I levels in growing cells and in the ECM secreted by confluent fibroblasts (Fig. 1A–C). TGFβ was no longer able to increase collagen I levels in medium containing 20% Gln (Fig. 1B). In medium containing 10% Gln, TGFβ-treated but not mock-treated fibroblasts

ceased to proliferate and produce collagen I (Fig. 1A–C). To validate these findings in fibroblasts relevant to cancer, we used primary pancreatic stellate cells (PSCs) and primary mammary fibroblasts (MFBs), the predominant mesenchymal cells that become activated and contribute to the desmoplastic stroma in PDAC or BRCA, respectively [18,19]. Glutamine titration experiments revealed a higher dependency of primary PSCs and MFBs compared to NIH-3T3 cells on glutamine for growth (Extended Data Fig. 1A, D). We therefore used "10% Gln" for NIH-3T3 cells and "20% Gln" for primary PSCs and MFBs as the "low Gln" condition in the following experiments. In 20% Gln, PSCs and MFBs were unable to proliferate and produce collagen I when treated with TGFβ (Extended Data Fig. 1A, B, D, E). In addition, TGFβ could no longer stimulate collagen accumulation in the ECM generated by confluent PSCs and MFBs when the glutamine concentration in the medium was reduced to 20% or lower (Extended Data Fig. 1C, F).

We next asked why collagen production in TGFβ-stimulated fibroblasts was impaired when the extracellular glutamine concentration was reduced. Based on a recent report suggesting that glutamine-tRNA is often uncharged when cells are cultured in low amino acid medium [20], we used a qPCR-based method to analyze the charging state of tRNAs for several non-essential amino acids (NEAAs) and leucine-tRNA as control. We observed a profound uncharging of glutamine-tRNA in TGFβ- but not mock-treated NIH-3T3 cells cultured in low Gln (Fig. 1D). Consistent with tRNA uncharging, we observed that fibroblasts stimulated with TGFβ in low Gln displayed phosphorylation of the kinase GCN2 (Fig. 1E), which is auto-phosphorylated upon binding to uncharged tRNAs and induces a reduction of bulk translation while at the same time upregulates translation of ATF4 to activate the integrated stress response [21]. Consistently, ATF4 was upregulated in TGFβ-stimulated fibroblasts in low glutamine, while bulk translation was reduced compared to control cells (Fig. 1E, F). These data suggest that an inability to maintain glutamine tRNA charging could lead to activation of GCN2 and reduced translation in fibroblasts treated with TGFβ in a low glutamine environment, resulting in a reduction of ECM synthesis. Glutamine-tRNA charging has been reported to be restored in proliferative fibroblasts by inhibiting glutaminase with the allosteric inhibitor CB839 [20]. However, CB839 treatment did not rescue GCN2 activation induced by TGFβ treatment in low Gln and only marginally increased collagen I protein levels (Fig. 1G), indicating that other fates of glutamine could also be limiting for collagen production.

Glutamine is a major anaplerotic substrate in proliferating cells [22] and in TGFβ-stimulated fibroblasts [11]. Notably, in addition to glutamine, free levels of most TCA cycle intermediates were substantially reduced in fibroblasts treated with TGFβ in low Gln, as were several TCA cycle related NEAAs including glutamate, aspartate, and asparagine (Fig. 1H). Asparagine and proline individually did not rescue the TGFβ-induced growth defect and collagen I depletion in low Gln (Extended Data Fig. 1G, H). However, high levels of cell-permeable glutamate (dm-Glu) but not proline (m-Pro) were sufficient to restore growth and collagen I levels in TGFβ-treated fibroblasts in low Gln (Fig. 1I, J). A cell-permeable version of the TCA cycle intermediate alpha-ketoglutarate (dm-αKG) was also able to rescue both growth and collagen I levels under these conditions (Fig. 1I, J). Dm-Glu and dm-αKG both rescued the TGFβ-induced depletion of TCA cycle intermediates and NEAAs and prevented GCN2 activation in low Gln medium (Fig. 1J; Extended Data Fig. 1I). PSCs and

MFBs cultured in low Gln also showed GCN2 phosphorylation when treated with TGFβ (Extended Data Fig. 1J, K). Consistently, analysis of tRNA charging under these conditions revealed uncharging of both glutamine- and aspartate-tRNA in PSCs (Extended Data Fig. 1L), and aspartate-tRNA in MFBs (Extended Data Fig. 1M). The additional uncharging of aspartate-tRNA in PSCs and MFBs treated with TGFβ in low Gln indicated that these cells were further limited in their ability to maintain the TCA cycle to support NEAA synthesis and collagen production. Consistent with this idea, supplementing TGFβ-treated PSCs and MFBs in low Gln with cell-permeable anaplerotic substrates or aspartate rescued collagen levels and GCN2 phosphorylation (Extended Data Fig. 1N, O).

Glutamine *de novo* synthesis can maintain collagen synthesis

In addition to being used as an anaplerotic substrate, αKG can be transaminated to glutamate, which can then be amidated by glutamine synthetase (encoded by *Glul*) to synthesize glutamine *de novo*. Glutamine *de novo* synthesis has been shown to be active in tumor-associated fibroblasts in ovarian and pancreatic cancer [23,24]. Given that TGFβ-treated NIH-3T3 cells and PSCs showed glutamine-tRNA uncharging in low Gln, we asked whether dm-αKG supplementation promotes collagen production by supporting glutamine *de novo* synthesis. Treatment with dm-αKG restored the charging of glutamine-tRNA in TGFβ-treated cells in low Gln, and this was blocked by methionine sulfoximine (MSO), an irreversible inhibitor of GLUL (Fig. 2A). Treatment with dm-αKG also suppressed GCN2 activation and promoted translation in TGFβ-treated cells in low Gln, which was dependent on glutamine *de novo* synthesis (Fig. 2B, C). In addition, the restoration of collagen levels by dm-Glu and dm-αKG in TGFβ-treated NIH-3T3 cells and PSCs in low glutamine was prevented by treatment with MSO (Fig. 2C–E; Extended Data Fig. 2A, B). To confirm these results genetically, we deleted *Glul* by CRISPR/Cas9. Deletion of *Glul* compromised fibroblast growth in low Gln in the absence of TGFβ (Extended Data Fig. 2C, D) and significantly reduced the ability of dm-αKG and dm-Glu to rescue the proliferation of TGFβ-treated cells (Extended Data Fig. 2C). In addition, *Glul* deletion almost completely blocked the increase of collagen I protein upon dm-αKG and dm-Glu supplementation in TGFβ-treated fibroblasts in low Gln containing medium (Fig. 2F). *Glul* deletion resulted in glutamine-tRNA uncharging, GCN2 activation and a reduction in protein translation in untreated fibroblasts cultured in low Gln (Fig. 2G–I). In addition, NIH-3T3 cells were unable to maintain collagen I synthesis when *Glul* was deleted or inhibited with MSO (Fig. 2I, J). Similar results were obtained in *Glul*-deleted PSCs (Extended Data Fig. 2E–G).

The requirement for GLUL to maintain cell proliferation and collagen production in fibroblasts cultured in low Gln in the presence or absence of TGFβ suggested that TGFβ treatment resulted in a dependency on glutamine for TCA cycle anaplerosis, indicating an inability to use other anaplerotic substrates. The other main anaplerotic substrate is pyruvate which can be converted to oxaloacetate by pyruvate carboxylase (PC). Some cancer cells can maintain growth via PC-mediated anaplerosis from pyruvate when glutamine-derived anaplerosis is limited *in vitro*, or in the tumor microenvironment *in vivo* [25–28]. To see if fibroblasts also used PC, we first analyzed PC mRNA (*Pcx* in mouse) and protein expression. PC transcript and protein levels were reduced by TGFβ treatment in all fibroblast types analyzed, despite other well-known TGFβ-responsive genes being induced

(Fig. 3A, B; Extended Data Fig. 3A–D). TGFβ treatment also reduced the repressive phosphorylation of the E1α subunit of the pyruvate dehydrogenase (PDH) complex, indicative of higher activity (Fig. 3B). To test whether the reduced expression of PC could be a direct effect of TGFβ signaling, we examined if there were binding sites for the TGFβ-induced transcriptional mediators SMAD2/3/4 around the putative promoter region and transcriptional start site (TSS) of human PC. Indeed, SMAD2/3/4 binding motifs were enriched within the analyzed regions ($P<0.0001$, Extended Data Fig. 3E). In addition, analysis of human SMAD4 chromatin-immunoprecipitation (ChIP)-sequencing data from the ENCODE project confirmed enrichment of SMAD4 at the putative *PC* promoter region and TSS (Extended Data Fig. 3E). Through CRISPR/Cas9-mediated deletion of *Smad4*, we confirmed that TGFβ-induced downregulation of PC protein was Smad4-dependent (Fig. 3C). We also analyzed PC expression in different subtypes of cancer-associated fibroblasts (CAFs) that have been described in PDAC [29], which revealed lower *PC* mRNA expression in TGFβ-driven myofibroblastic CAFs (myCAFs) compared to IL1-driven inflammatory CAFs (iCAFs) (Extended Data Fig. 3F, G).

Pyruvate carboxylase activity is suppressed by TGFβ

To test whether TGFβ treatment also alters PC activity, we traced the fate of fully [^{13}C]-labeled glucose ([U-^{13}C] Glc) into TCA cycle intermediates and related NEAAs, focusing on three carbon labeling (m+3) which can be used as a surrogate for PC activity (Fig. 3D). Culture of control fibroblasts in low Gln increased m+3 labeling of TCA cycle intermediates and NEAAs from [U-^{13}C] Glc (Fig. 3E), indicating an increase in the relative contribution of PC to the pool of these metabolites. In addition, m+5 labeled glutamate and citrate, reflective of the combined activity of PC and PDH, were increased upon culture in low Gln (Fig. 3E). In contrast, TGFβ treatment reduced m+3 and/or m+5 labeling of the metabolites analyzed, in both high and low Gln containing medium, while m+2 labeling of citrate, indicative of PDH activity, was increased (Fig. 3E), consistent with reduced PDH phosphorylation in TGFβ-treated cells (Fig. 3B). Similar results were obtained in PSCs (Extended Data Fig. 3H). In addition, TGFβ reduced m+3 labeling of aspartate and glutamate/glutamine that are incorporated into cellular protein (Extended Data Fig. 3I). To further support these findings, we performed tracing experiments with [3,4-^{13}C] Glc. This tracer is metabolized to [1-^{13}C] pyruvate and yields one-carbon labeled TCA cycle intermediates when carboxylated via PC, while the label is lost when decarboxylated via PDH (Fig. 3F) [25]. Consistent with the above results, m+1 labeling of aspartate, malate, and citrate increased when fibroblasts were cultured in low Gln, and this increase was suppressed by TGFβ treatment, indicative of lower PC activity (Fig. 3G, H). Similarly, PC activity increased in PSCs cultured in low Gln but was suppressed in the presence of TGFβ (Extended Data Fig. 3J, K).

To confirm the influence of *PC* in the inability of TGFβ-stimulated fibroblasts to grow or produce collagen when cultured in low Gln containing medium, a *PC* cDNA was introduced in NIH-3T3 cells and PSCs. Both the absolute levels, and the m+3 and m+5 labeling of TCA cycle intermediates and NEAAs from [U-^{13}C] Glc was increased in cells expressing *PC* cDNA growing in 10% Gln in the presence of TGFβ (Fig. 3I, J). *PC* overexpression increased protein translation in TGFβ-treated cells cultured in low Gln, and this increase

was blocked by the GLUL inhibitor MSO (Fig. 3K), indicating that PC-supported protein translation depends on glutamine *de novo* synthesis. Expression of *PC* cDNA was also sufficient to increase cell growth and collagen I protein when TGFβ-treated cells were cultured in low glutamine (Fig. 3L, M; Extended Data Fig. 3L).

PC anaplerosis is required for collagen synthesis in low Gln

In the absence of TGFβ, fibroblasts grown in low Gln medium were able to maintain collagen production (Fig. 1). We next asked if collagen synthesis under these conditions required PC. Fibroblasts grown in low Gln were unable to accumulate collagen I when *PC* was deleted, and these cells had increased GCN2 phosphorylation that was accompanied by accumulation of ATF4 (Fig. 4A). In contrast, there was no change in collagen I accumulation in comparison to wild-type cells when *PC*-deleted cells were cultured in high Gln (Extended Data Fig. 4A). Similar results were obtained when *PC* was deleted in PSCs and MFBs (Extended Data Fig. 4B, C). Importantly, reduced levels of collagen were also observed in the ECM produced by confluent PSCs and MFBs with *PC* deletion cultured in low Gln (Extended Data Fig. 4D). To test whether the inability of *PC*-deleted cells to synthesize collagen I was due to the lack of anaplerotic input, we supplemented these cells with dm-αKG or dm-Glu. Both dm-αKG and dm-Glu increased collagen I levels in *PC*-deleted cells cultured in low Gln (Fig. 4B; Extended Data Fig. 4E). Indeed, TCA cycle intermediates and related NEAAs were depleted in *PC*-deleted cells cultured in low glutamine (Fig. 4C). To confirm that *PC* deletion impairs TCA cycle anaplerosis from glycolytic carbon, glucose metabolic tracing studies were performed comparing control and *PC*-deleted cells. Control fibroblasts grown in low Gln increased their m+3 and m+5 labeling of TCA cycle intermediates and related NEAAs from [U-^{13}C] Glc compared to cells grown in high Gln (Fig. 3E, Fig. 4D), and this increase was suppressed when *PC* was deleted (Fig. 4D). Furthermore, *PC* deletion reduced m+1 labeling of aspartate and citrate from [3,4-^{13}C] Glc in both high and low Gln (Extended Data Fig. 4F). While some pyruvate carboxylation activity remained in *PC*-deleted cells, possibly due to the activity of malic enzyme [27], only PC-dependent pyruvate carboxylation increased upon culture in low Gln (Extended Data Fig. 4F).

In high Gln, *PC* deletion if anything promoted cell growth, while in low Gln there was a reduction in cell growth upon *PC* deletion (Extended Data Fig. 4G). Similar results were obtained in PSCs and MFBs (Extended Data Fig. 4H, I). To further support these findings, we used the glutaminase inhibitor CB839 to block TCA cycle anaplerosis from glutamine. CB839 treatment alone did not affect collagen I levels in cells cultured in full medium (Fig. 4E), but increased m+3 labeling of TCA cycle intermediates and related NEAAs from [U-^{13}C] Glc (Fig. 4F), indicative of increased anaplerosis via PC. Consistent with this, m+1 labeling of aspartate and pyruvate carboxylation activity from [3,4-^{13}C] Glc was increased in cells treated with CB839 (Fig. 4G). To test whether PC-mediated anaplerosis supports collagen synthesis when anaplerosis from glutamine is inhibited, we treated *PC*-deleted cells with CB839. In the absence of *PC*, CB839 treatment resulted in reduced collagen I levels (Fig. 4H). Thus, PC-mediated TCA cycle anaplerosis supports collagen production when anaplerosis from glutamine is impaired.

Our glucose metabolic tracing studies indicated that *PC*-deleted cells are impaired in their ability to use glucose-derived carbon for TCA cycle anaplerosis and the synthesis of NEAAs including glutamine (Fig. 4D, Extended Data Fig. 4F). This suggested that PC-mediated anaplerosis could maintain collagen I levels at least in part by supporting glutamine *de novo* synthesis. To test this, *PC*-deleted cells cultured in low Gln and supplemented with dm-aKG were treated with the GLUL inhibitor MSO. In the presence of MSO, dm-aKG was unable to restore collagen I levels in cells with *PC* deletion (Fig. 4I). Furthermore, *PC*-deleted cells cultured in low Gln medium were enriched for a gene expression signature characteristic of amino acid deprived cells (Fig. 4J), which was consistent with a selective uncharging of glutamine- and/or aspartate-tRNA (Fig. 4K; Extended Data Fig. 4J) and a reduced translation rate (Fig. 4L).

As loss of *PC* resulted in changes in gene expression upon culture in low Gln, we asked whether the impairment in collagen synthesis was also present at the transcriptional level. Indeed, *Col1a1* mRNA was downregulated in *PC*-deleted cells cultured in low Gln (Fig. 5A). This effect was also observed in PSCs and MFBs (Extended Data Fig. 4K). Changes in metabolite availability can influence gene expression by impacting the deposition and removal of chromatin modifications [30]. Histone acetylation is associated with actively transcribed genes and is controlled in part by the availability of citrate-derived acetyl-CoA. Reduced citrate levels in *PC*-deleted cells cultured in low Gln (Fig. 4C) suggested that histone acetylation could be impaired in these cells. To test this, we performed ChIP-qPCR, which showed that levels of acetylated H3K27 (H3K27ac), a mark associated with active enhancers, were significantly reduced at the distal *Col1a1* enhancer in *PC*-deleted cells cultured in low Gln, but not at control loci (Fig. 5B, Extended Data Fig. 4L). H3K27 can either be acetylated or methylated, and consistent with reduced H3K27ac, the repressive trimethylated H3K27 (H3K27me3) histone modification was enriched across two enhancer and two promoter regions of the *Col1a1* locus in *PC*-deleted cells cultured in low Gln, but not at control loci (Fig. 5C; Extended Data Fig. 4M). Based on these results, we hypothesized that addition of an alternative anaplerotic substrate would promote *Col1a1* mRNA expression when *PC* is lost. Indeed, supplementation with dm-αKG or dm-Glu rescued *Col1a1* mRNA expression in *PC*-deleted cells cultured in low Gln (Fig. 5D; Extended Data Fig. 4N), which was independent of glutamine *de novo* synthesis (Extended Data Fig. 4O). The expression of most collagen genes was downregulated in *PC*-deleted cells compared to control cells cultured in low Gln containing medium (Fig. 5E), indicating a general repression of collagen transcription when *PC* is lost.

Lactate supports collagen synthesis via PC in low Glc/Gln

The above data demonstrate that when extracellular glutamine concentrations are low, collagen production in fibroblasts can be maintained by PC-mediated anaplerosis from glycolytic carbon. However, glucose levels are also often reduced in tumors [15,17], indicating that glucose-derived pyruvate for PC-mediated TCA cycle anaplerosis could be limiting *in vivo*. Indeed, fibroblast production of collagen I progressively declined when the concentration of extracellular glucose was reduced in low Gln containing medium (Fig. 6A, Extended Data Fig. 5G), raising the question of how fibroblasts support TCA cycle anaplerosis for collagen synthesis *in vivo*.

While glutamine and glucose availability can be limited in tumors, lactate is the most consistently elevated metabolite in human tumors [31]. To test whether fibroblasts can use lactate for TCA cycle anaplerosis, we performed metabolic tracing studies with uniformly labeled lactate ([U-^{13}C] Lac). Consistent with previous studies in ovarian tumor-associated fibroblasts [23], in the presence of extracellular lactate, the contribution of glucose to the cellular pyruvate pool was reduced, and the majority of pyruvate was derived from extracellular lactate, even when extracellular glucose and glutamine were abundant (Fig. 6B; Extended Data Fig. 5A). In fibroblasts supplemented with lactate, lactate-derived pyruvate preferentially contributed to the TCA cycle and related NEAAs compared to glucose-derived pyruvate (Extended Data Fig. 5A), which is consistent with metabolic flux analysis in whole organs [32]. We observed that the utilization of lactate-derived pyruvate via PC (m+3) increased in low Gln containing medium (Fig. 6B), indicating that lactate-derived pyruvate could act as anaplerotic substrate. Consistent with this, m+1 labeling of aspartate, malate and citrate and pyruvate carboxylation activity from [1-^{13}C] Lac was elevated under low Gln culture conditions (Fig. 6C, D).

We therefore asked whether extracellular lactate could support collagen production when both glutamine and glucose concentrations were reduced. Indeed, lactate supplementation to fibroblasts cultured in low glutamine and low glucose increased collagen I levels (Fig. 6E). Pyruvate was more potent than lactate; however, at concentrations relevant *in vivo* (10 mM lactate, 0.1 mM pyruvate), only lactate supplementation increased collagen I levels under low glutamine and low glucose conditions (Fig. 6E). This effect was dependent on lactate import via MCT1 and conversion to pyruvate via LDH (Fig. 6F, Extended Data Fig. 5B). To test whether lactate supported TCA cycle anaplerosis via PC, we performed [U-^{13}C] Lac tracing in cells with *PC* deletion cultured in low glutamine. While there was no difference in pyruvate labeling from lactate in *PC*-deleted cells, lactate carbon could no longer be used for TCA cycle anaplerosis in the absence of *PC* (Fig. 6G). This was confirmed using [1-^{13}C] Lac as a tracer (Extended Data Fig. 5C, D). Consistent with these results, the ability of extracellular lactate to rescue collagen I in cells cultured in low glutamine and low glucose was PC-dependent (Fig. 6H). In addition, lactate increased collagen levels in the ECM produced by confluent fibroblasts in low glutamine and low glucose containing medium in a PC-dependent fashion (Extended Data Fig. 5E, F). Tracing of [U-^{13}C] Lac into hydrolyzed ECM proteins revealed that lactate carbon directly contributed to collagen via PC (Fig. 6I). Similar results were obtained in PSCs (Extended Data Fig. 5G–L).

Fibroblast PC supports tumor fibrosis and growth

Having established that PC-mediated anaplerosis supports collagen production in fibroblasts under conditions reminiscent of a nutrient-poor tumor microenvironment, we next asked how PC-regulated collagen levels in fibroblast-derived ECM affect cancer cells. To this end, we used a three-dimensional (3D) spheroid culture system, in which KPC mouse PDAC cells were first plated on ultra-low attachment plates to form spheroids that were then transferred onto ECM on which cells start to grow out of the spheroid and proliferate. We first cultured KPC spheroids on a synthetic ECM generated by gelating increasing concentrations of collagen I with Matrigel, a basement membrane mix containing a variety of matrix proteins (Extended Data Fig. 6A). Spheroid outgrowth correlated with the

concentration of collagen I in the synthetic ECM (Extended Data Fig. 6B). Next, KPC spheroids were cultured on PSC-derived ECM that was produced in the presence of TGFβ and media containing 100% or 10% Gln (Extended Data Fig. 6C). ECM produced in 10% Gln by TGFβ-stimulated PSCs was depleted of collagen I but not of fibronectin (Extended Data Fig. 6C), another prominent ECM protein. Spheroid outgrowth was significantly reduced when cultured on ECM that was produced by TGFβ-treated PSCs in 10% Gln compared to 100% Gln (Extended Data Fig. 6D, E). We then used untreated PSCs with deletion of *PC* or *Glul* to prepare ECM in the presence of 20% Gln (Fig. 7A). ECM generated by *PC*- or *Glul*-deleted PSCs under these conditions had a substantially lower collagen I content compared to control cells but was similarly enriched in fibronectin (Fig. 7A). When KPC spheroids were cultured on ECM generated by *PC*- or *Glul*-deleted PSCs under 20% Gln, their outgrowth was reduced compared to the outgrowth on ECM produced by control PSCs under these conditions (Fig. 7B, C). It has been reported that fibroblast-derived glutamine can support the survival of PDAC cells under glutamine limitation [24]; however, both control and *Glul*-deleted PSCs were similarly able to promote survival of KPC cells in the absence of extracellular glutamine (Extended Data Fig. 6F).

Next, we asked whether fibroblast *PC* and *Glul* are relevant for collagen levels and tumor growth *in vivo*. To this end, KPC cells were injected subcutaneously into the flanks of nude mice, either alone or along with PSCs expressing either a control, *PC* or *Glul* sgRNA (Fig. 7D). The presence of PSCs promoted tumor growth substantially (Fig. 6D), as previously reported [19]. While *PC*- or *Glul*-deleted PSCs retained the ability to enhance the growth of KPC-derived tumors, tumor growth was significantly reduced compared to co-injection with control PSCs (Fig. 7D). Intratumoral fibrosis was lower in tumors formed by KPC cells that were co-injected with *PC* or *Glul*-deleted PSCs compared to control PSCs (Fig. 7E, F; Extended Data Fig. 6G–I), while the levels of αSMA, a marker for activated fibroblasts, were similar across tumors (Fig. 7G; Extended Data Fig. 6J, K). Co-injection of PSCs also promoted the growth and increased the collagen content of KPC-derived tumors in immunocompetent, syngeneic mice in a *PC*-dependent fashion (Fig. 7H, I).

We then assessed the ability of fibroblast-PC to regulate tumor growth and collagen content in a syngeneic BRCA co-injection model (Fig. 7J). Co-injection of MFBs promoted tumor growth of DB7 breast cancer cells in wildtype mice (Fig. 7J), and deletion of *PC* in MFBs with two different sgRNAs significantly reduced the growth of co-injected tumors (Fig. 7J). The beneficial effect of MFBs on tumor growth was prominent at early time points after co-injection and was similar to the tumor-promoting effect of Matrigel (Extended Data Fig. 6L). This raised the possibility that the growth of DB7 tumors could be supported by the matrix proteins secreted by MFBs. Consistent with this, co-injection of MFBs substantially increased the collagen content of DB7 allograft tumors after engraftment (Fig. 7K–M, Extended Data Fig. 6M). *PC* deletion in MFBs resulted in a more than 50% reduction of tumor collagen levels compared to co-injection of control MFBs (Fig. 7K–M). Thus, fibroblast PC is required for collagen production in the tumor microenvironment.

Discussion

The ability of fibroblasts to synthesize ECM is critical for wound healing. Fibroblast ECM synthesis can also be coopted by cancer cells to support tumor cell growth in solid tumors such as BRCA and PDAC. In such tumors, the chronic activation of fibroblasts to produce excessive amounts of ECM can modulate many of the hallmarks of cancer [7]. In this study, we sought to understand how fibroblasts maintain ECM production under nutrient poor conditions reported to be present in the tumor microenvironment. The present results demonstrate that PC-mediated TCA cycle anaplerosis is a critical regulator of ECM production in tumors.

PC is a widely expressed mitochondrial enzyme that catalyzes the carboxylation of pyruvate to oxaloacetate and as such provides a mechanism to replenish TCA cycle intermediates that are being consumed in support of macromolecular synthesis [33]. PC has been well studied in the liver, where its activity is critical for gluconeogenesis, the urea cycle and antioxidant capacity [34,35]. While PC appears to be dispensable for normal and cancer cell growth under standard culture conditions, PC has also been shown to be required to support cancer cell growth *in vivo* [26–28]. Our work suggests that PC is also critical to the stromal cells in the tumor microenvironment and to their role in supporting cancer cell growth.

We find that PC-mediated TCA cycle anaplerosis increases in fibroblasts when glutamine-dependent anaplerosis is impaired, consistent with studies in cancer cells [25]. Mechanistically, our data support a model in which under low glutamine conditions, PC-mediated anaplerosis maintains sufficient TCA cycle activity to sustain fibroblast growth and protein translation when anabolic precursors such as αKG are diverted into the synthesis of NEAAs. Interestingly, the αKG-derived salt ornithine alpha-ketoglutarate is known to improve wound healing in patients with injuries and burns [36]; conditions under which glutamine levels drop significantly [14]. Consistent with the present findings, it has been suggested that αKG's beneficial effects on wound healing are mediated at least in part through the replenishment of glutamine and other NEAAs pools [37].

In addition to supporting protein translation, the present data also show that PC-mediated TCA cycle anaplerosis supports transcription of collagens under low glutamine conditions. This correlated with the ability of PC-mediated anaplerosis to maintain H3K27 acetylation at the *Col1a1* locus. H3K27 acetylation was recently shown to regulate *Col1a1* transcription in a fibrosis model [38]. Our finding that *Col1a1* mRNA expression is reduced in *PC*-deleted cells cultured in low glutamine is consistent with this model. Reciprocally, repressive H3K27 trimethylation at the *Col1a1* locus was increased in cells with *PC* deletion in low glutamine medium, indicating that PC-mediated anaplerosis contributes to regulating the balance of histone acetylation and methylation. These findings support the emerging concept that the gene expression program of tumor-associated fibroblasts can be regulated by metabolism-driven epigenetic reprogramming [39,40]. Unlike the recently reported immunosuppressive role of selective deletion of *Col1a1* in PDAC [41], the dependence of fibroblasts on PC is not restricted to *Col1a1* expression but is also detected in the expression of other collagens and ECM proteins. Thus, PC is required to produce the collective mix of proteins that contribute to the ECM by supporting fibroblast transcription and translation

and may therefore also be required for fibroblast-mediated tumor support in more complex model systems.

We then investigated the potential source of the pyruvate that is carboxylated by fibroblast-PC to support tumor desmoplasia *in vivo*. Our findings suggest that when both extracellular glutamine and glucose concentrations are low, lactate can be used to maintain collagen production in fibroblasts in a PC-dependent fashion. Lactate concentrations in healing wounds can rise to more than 10 mM, and comparable lactate accumulation in the tumor microenvironment has been reported across studies and cancer types [31]. Lactate is oxidized in wounds and can fuel the TCA cycle in whole tumors [32,42], but so far it remains unclear which cell type in the tumor microenvironment utilizes lactate. Tumor-associated fibroblasts have been reported to secrete lactate under standard culture conditions [43,44] and are thus considered to contribute to, rather than utilize the lactate accumulating in tumors. However, the transport of lactate across the plasma membrane is dependent on its intra- and extracellular concentration and is coupled to the proton gradient, and these factors can differ in tumors and culture systems. The present data indicate that lactate can be taken up by fibroblasts and contribute to the cellular pyruvate pool, independent of the concentration of glucose and glutamine in the culture media. This is consistent with the rapid exchange flux of lactate and pyruvate which has also been observed *in vivo* [32,45]. When TCA cycle anaplerosis from glutamine is limited, lactate-derived pyruvate can be used for anaplerosis in a PC-dependent fashion. Lactate consumption and contribution to the TCA cycle has also been reported in ovarian cancer-associated fibroblasts and in mesenchymal stem cells [23,40]. While differences in fibroblasts across tissues might exist, these data suggest that fibroblasts can contribute to lactate consumption observed in tumors and might utilize lactate accumulating in tumors and healing wounds to fuel ECM synthesis. Based on the recently reported effects of lactate on other stromal cell types, our data further support the idea that lactate accumulation in the tumor microenvironment can promote a stromal regenerative response [13].

Glucose and glutamine are among the highest consumed nutrients by proliferating cells [22]. As a consequence, glucose and glutamine concentrations in commonly used cell culture media (20 mM and 2 mM, respectively, in this study) are about four-fold higher than found in human plasma (5 mM and 0.5 mM) [12]. Our finding that 0.4 mM glutamine (20% Gln) can be limiting for primary fibroblast collagen production *in vitro* indicates that physiological glutamine levels might be limiting for ECM synthesis. However, unlike in standard cell culture experiments, nutrients are constantly exchanged through the vasculature in healthy tissues *in vivo*, and are likely maintained at a concentration supportive of essential cellular functions, including ECM production by fibroblasts. In contrast, fresh wounds and most tumor types are poorly vascularized, resulting in reduced nutrient delivery and accumulation of metabolic waste products [46]. Thus, the cell culture experiments performed in this study partially mimic the stromal regenerative response observed in many tumors and healing wounds [13]. Impairments in functional vasculature, coupled with the high proliferative activity of cancer cells, generally led to the assumption that glucose and glutamine are depleted in the microenvironment of tumors, relative to levels in plasma and healthy tissues, while lactate accumulates substantially. The reduction of glucose and glutamine and accumulation of lactate have been confirmed in extracts of various tumor types, tumor

models and species [15–17,31]. The requirement of PC-mediated TCA cycle anaplerosis for collagen production only under glutamine-deprived conditions *in vitro* suggests that in the tumor models studied here, glutamine levels are at least at some point limiting for fibroblast collagen synthesis. Nevertheless, given the dependency on PC for tumor growth across cancer models that is not observed in standard cell culture conditions [26–28], we cannot rule out that other aspects only present *in vivo* alter the requirement for PC in fibroblasts.

TGFβ-mediated stimulation of fibroblast growth and matrix production has long made it a target for strategies to impair fibrotic reactions. However, here we find that in fibroblasts, TGFβ-stimulated collagen synthesis depends on glutamine availability. While TGFβ/Smad4 signaling promotes anaplerosis from glutamine [11], it suppresses anaplerosis from pyruvate via PC, resulting in depletion of TCA cycle intermediates when extracellular glutamine is limiting. Thus, TGFβ renders the TCA cycle dependent on anaplerosis from glutamine. The resulting coupling of matrix production to glutamine availability in TGFβ-stimulated fibroblasts supports collagen synthesis when glutamine is abundant, inducing fibroblasts to store glutamine-derived carbon and nitrogen in the form of highly reduced proline as part of collagen proteins. When glutamine becomes limiting, this coupling could preserve glutamine for parenchymal cells such that organ-specific functions can be maintained. Under such conditions, cancer cells can digest and take up previously laid down ECM proteins to support NEAA biosynthesis and energy homeostasis [47]. Thus, fibroblast-derived ECM could serve as sink for carbon, nitrogen and electrons in the tumor microenvironment. As fibroblasts constantly remodel the ECM, this sink might also be used by tumor-associated fibroblasts themselves [48]. Under physiological conditions of a healing wound, the TGFβ-induced coupling of fibroblast collagen production to the glutamine supply could be important to prevent connective tissue regeneration before vascularization is restored.

The regulation of PC expression by TGFβ also suggest that inhibiting TGFβ receptor signaling could potentially increase tumor-associated fibroblast production of collagen through derepressing *PC* expression and thereby enhance desmoplasia. An interesting correlate of this is that TGFβ-induced repression of *PC* is Smad4-dependent. Lau et al. (2020) recently reported that in PDAC, tumor cell growth in 3D culture or xenografts is dependent on PC activity. This raises the intriguing possibility that by preventing TGFβ-induced suppression of PC, *SMAD4* deletion that is present in 50% of human PDAC confers a metabolic advantage to PDAC cells when glutamine is limited.

In conclusion, our study establishes TCA cycle anaplerosis as a critical determinant for ECM production in fibroblasts. Specifically, we provide evidence that PC-mediated anaplerosis in tumor-associated fibroblasts contributes to tumor fibrosis and growth. This requirement for PC expression only when glutamine levels are low could represent a unique vulnerability of fibroblasts that when targeted therapeutically might allow reducing tumor desmoplasia selectively in glutamine-depleted tumors while not affecting the synthesis of ECM in normal tissue.

Methods

Cell culture

NIH-3T3 cells were obtained from ATCC (CRL-1658). 293T cells were obtained from ATCC (CRL-3216). PSCs were isolated from C57BL/6 mice by differential centrifugation as previously described [49] and their mesenchymal origin was validated by analyzing the expression of various mesenchymal and epithelial markers. MFBs were isolated from FVB/N mice by differential centrifugation as previously described [50]. DB7 mouse breast cancer cells were obtained from Alexander Borowsky (University of California Davis Comprehensive Cancer Center, Sacramento, CA) through an MTA to OSU. KPC (*Kras*$^{LSL\text{-}G12D}$;*Trp53*$^{LSL\text{-}R272H}$;Pdx1-Cre) mouse PDAC cells were a gift from Scott Lowe (MSKCC). All cells were cultured at 37°C in 5% CO_2 and 20% O_2 and were maintained in DMEM (25 mM D-glucose, 2 mM L-glutamine) supplemented with 10% FBS (Gemini), 100 units/ml penicillin and 100 μg/ml streptomycin. Primary PSC and MFB cells were kept in culture for no more than 10 passages. Experiments with iCAFs and myCAFs were performed as previously described [29]. In brief, qPSCs were generated by culturing PSCs in a dome of GFR Matrigel (Corning) in DMEM; iCAFs were generated by culturing PSCs in a dome of GFR Matrigel in DMEM conditioned by KPC cells for 48h; myCAFs were generated by monolayer culture of PSCs. Differentiation was validated by analyzing the expression of iCAF/myCAF markers [29]. For experiments with different glutamine concentrations, cells were seeded in regular DMEM and the medium was changed 5–6h later or the following day to glucose- and glutamine-free DMEM supplemented with 10% dialyzed FBS (Gemini) and 20 mM D-glucose, 2 mM L-glutamine (100%), 0.4 mM L-glutamine (20%) or 0.2 mM L-glutamine (10%). All media were prepared by the Media Preparation Facility at MSKCC. Cells were verified as mycoplasma-free by the MycoAlert Mycoplasma Detection Kit (Lonza).

Growth experiments

0.2×10^5 cells/well were plated in 24-well culture plates and media was changed and treatments started 5–6h later. Cell numbers at the start of treatment (d0) and one, two and three days later were counted using the Multisizer 4e (Beckman) and normalized to the cell number at d0. In co-culture assays, a fraction of the cell population was analyzed by flow cytometry for GFP expression, and the rest counted with the Multisizer 4e. The number of KPC-GFP cells was determined by multiplying the fraction of GFP+ cells with the total number of cells. The gating strategy is shown in Extended Data Fig. 7B.

Chemicals

TGFβ−1 was purchased from Peprotech; Amino acids (L-asparagine, L-glutamine, proline), cell-permeable metabolites (L-proline methyl ester hydrochloride, L-glutamic acid dimethyl ester hydrochloride, dimethyl 2-oxoglutarate), sodium lactate and L-methionine sulfoximine were purchased from Sigma; CB839 was purchased from Selleck; AZD3965 was purchased from MedChem Express; sodium oxamate was purchased from Cayman Chemical; stable isotopes ([U-^{13}C] glucose, [3,4-^{13}C] glucose, [U-^{13}C] lactate, [1-^{13}C] lactate) were purchased from Cambridge Isotope Laboratories. An equivalent amount of solvent (DMSO or water) was added to control samples to control for any solvent-based effects.

Ectopic gene expression and CRISPR/Cas9 mediated gene deletion

Human *PC* cDNA plasmid was obtained from DNASU (HsCD00436386). Guide RNAs targeting murine *Glul* and *PC* were designed using GuideScan (http://www.guidescan.com/) and cloned into pLentiCRISPRv2 (Addgene 52961). The following guide sequences were used: TCGCGCCTACGATCCCAAGG (*Glul* sg4), TGGGATCGTAGGCGCGAATG (*Glul* sg6), GCACGCACGAAACACTCGGA (*PC* sg1), TAGGCTTATACTCCAGACGC (*PC* sg2), AAGTTCCAAACAGTTCGAGG (*PC* sg4), GTTCATTGGTCCAAGCCCAG (*PC* sg5). *Smad4* and Rosa26 targeting guides (Ctrl sg) were described before [11]. Lentiviral particles were produced in 293T cells by using psPAX2 and pCMV-VSV-G packaging plasmids (Addgene). Viral supernatant was collected after 48h, passed through a 0.45 μm nylon filter and used to transduce NIH-3T3 cells in the presence of 8 μg/mL polybrene (Sigma) overnight. Cells were subjected to puromycin (2 μg/mL, Sigma) or blasticidin (10 μg/mL, Invivogen) antibiotic selection the following day. Polyclonal cell populations were used for the experiments.

Western blot

Lysates were generated by incubating cells or ground tumors in RIPA buffer (Millipore). 20–30 μg of cleared lysate were analyzed by SDS-PAGE as previously described [11]. The following primary antibodies were used: Vinculin (1:5,000 dilution; Sigma, V9131), β-Actin (1:5,000; Sigma, A5441), Collagen I (1:500; Abcam, ab21286), Fibronectin (1:1,000; Abcam, ab2413), Smad4 (1:200; Santa Cruz, sc-7966), Smad2 p-S465/467 (1:1,000; Cell Signaling, 3108S), Smad2/3 (1:1,000; Cell Signaling, 3102S), GCN2 p-T899 (1:1,000; Abcam, ab75836), GCN2 (1:1,000; Cell Signaling, 3302S), ATF4 (1:200; Santa Cruz, sc-200), PC (1:1,000; Novus, NBP1–49536), S6K (1:1,000; Cell Signaling, 2708S), GLUL (1:1,000; Sigma, G2781), SMA (1:1,000; Millipore, CBL171). The following secondary antibodies were used: anti-rabbit HRP (1:5,000; GE, NA934V), anti-mouse HRP (1:5,000; GE, NA931). Quantification of band intensities of collagen I relative to β-actin or vinculin in tumor allograft experiments was performed with Image Lab software v6.0 (Bio-Rad).

Translation assays

Cells were treated as indicated and incubated with 20 μM O-propargyl-puromycin (OPP, Thermo Scientific) for the last 1h of the experiment. Cells were harvested by trypsinization and fixed with methanol at −20°C, followed by permeabilization with 0.5% Triton X-100 in PBS. Cells were stained using the Click-iT Plus Alexa Fluor 647 Picolyl Azide Toolkit (Thermo Scientific) according to the manufacturer's instructions and analyzed by flow cytometry. The gating strategy is shown in Extended Data Fig. 7A.

ECM extraction and collagen staining

Culture plates were coated with 0.1% gelatin (Sigma) and treated with 1% glutaraldehyde (Sigma) and 1 M ethanolamine (Sigma). Confluent NIH-3T3 cells, MFBs or PSCs were grown for six days on coated plates in the presence of 50 μM sodium ascorbate (Sigma) and treated as indicated, and the medium was replaced every other day. Plates were decellularized with 20 mM ammonium hydroxide/0.5% Triton-X 100 for 5 min on a rotating platform. Three times the volume of PBS was added, and ECM was equilibrated overnight

at 4°C, followed by four additional PBS washes. For western blot, pre-heated sample buffer supplemented with 1 mM DTT was added, ECM was scraped off and boiled, and proteins were separated by SDS-page followed by immunoblotting. To measure collagen abundance, fibroblast-derived ECM was stained with the Picro Sirius Red Stain Kit (Abcam) according to the manufacturer's instructions. The stain was extracted with 0.1 M NaOH and optical density was measured at 550 nm using a microplate reader. Differences in cell number were controlled for by growing cells on separate plates under the same experimental conditions.

Spheroid outgrowth

Spheroids were generated by plating 1×10^4 KPC cells in ultra-low attachment spheroid microplates (Corning). The next day, spheroids were transferred to 24-well plates containing synthetic ECM or fibroblast-derived ECM using a P1000 pipette at one spheroid per well. Synthetic ECM was generated by gelating different concentrations of high-concentration rat tail collagen I (Corning) and growth-factor reduced Matrigel (Corning) at a final concentration of 20% in a 37°C incubator for 1h. Spheroids were cultured on top of fibroblast-derived or synthetic ECM in DMEM with 10% FBS and were imaged 2–3h after transfer on ECM (d0) and the three following days with a Zeiss AxioCam microscope. Spheroid area, including outgrowing cells, was quantified manually in Fiji (v2.0).

Stable isotope labeling and metabolite extraction

Cells were plated in 6-well cell culture plates at a concentration aimed to reach $0.5–1\times10^6$ cells at the time of harvest. For quantification of relative metabolite abundance, cells were cultured glutamine-free DMEM containing different concentrations of L-glutamine and supplemented with 10% dialyzed FBS and in some experiments were treated with TGFβ for 48h. For the [U-^{13}C] and [3,4-^{13}C] glucose tracing experiments, cells were cultured as above, and in the last 8h media was replaced with DMEM without D-glucose and L-glutamine supplemented with 2 mM or 0.2 mM L-glutamine and 10 mM [U-^{13}C] or [3,4-^{13}C] D-glucose (Cambridge Isotope Laboratories) and 10% dialyzed FBS. For the [U-^{13}C] and [1-^{13}C] lactate tracing experiments, cells were cultured in 2 or 0.2 mM L-glutamine, 10 or 1 mM D-glucose in the presence or absence of 10 mM sodium lactate, and in the last 8h media was replaced with DMEM without D-glucose and L-glutamine supplemented with 2 mM or 0.2 mM L-glutamine, 10 or 1 mM D-glucose, 10 mM [U-^{13}C] or [1-^{13}C] sodium lactate (Cambridge Isotope Laboratories) and 10% dialyzed FBS. For relative quantification of metabolites by GC-MS, cells were washed briefly with PBS, which was then fully aspirated and metabolism was quenched by immediately adding 1 mL of 80:20 methanol:water stored at −80°C containing 20 μM deuterated 2-hydroxyglutarate (d5–2HG) as an internal standard. For stable isotope tracing experiments, metabolism was quenched without the PBS washing step by adding 1 mL of 80:20 methanol:water as above. After overnight incubation at −80°C, the resulting extracts were scraped on dry ice, transferred into a 1.5 mL centrifuge tube, and centrifuged at 20,000 g for 20 min at 4°C. The supernatants were collected in clean tubes and dried in a vacuum evaporator (Genevac EZ-2 Elite) for 2h.

Stable isotope labeling of cellular protein and ECM

For [U-^{13}C] glucose tracing into proteinogenic amino acids, cells were cultured in 10% Gln in the presence or absence of TGFb for 48h. In the last 24h, the media including all treatments was replaced with DMEM without L-glutamine and D-glucose and supplemented with 0.2 mM L-glutamine and 10 mM [U-^{13}C] D-glucose (Cambridge Isotope Laboratories) and 10% dialyzed FBS. For [U-^{13}C] lactate tracing into ECM, confluent cells were cultured in 10% Gln in the presence of 10 mM [U-^{13}C] sodium lactate for 6 days. The media was replaced every other day. ECM was decellularized as described above. Cells and ECM were washed with PBS, and proteins were precipitated with methanol:chloroform:water (1:1:1). The interphase was washed with methanol, and the dried pellet was subjected to acid hydrolysis with 6N HCl and incubation at 95°C for 16h. Samples were cooled to room temperature and centrifuged at 20,000 g for 10 min. The cleared supernatant was dried in a vacuum evaporator (Genevac EZ-2 Elite) for 2h, and abundance of aspartate, glutamate/glutamine or hydroxyproline isotopologues was measured by GC-MS as described below.

Measurement of hydroxyproline levels in tumors

Flash frozen tumors were ground to a powder in a cryocup grinder (BioSpec) cooled with liquid nitrogen. Acid hydrolysates were generated from aliquots of 5–10 mg ground tumor by addition of 6 N HCl (100 μL/mg) and incubation at 95°C for 16h. Samples were cooled to room temperature and centrifuged at 20,000 g for 10 min. 100 μL supernatant was dried in a vacuum evaporator (Genevac EZ-2 Elite) for 2h, and hydroxyproline levels were measured by GC-MS as described below.

Mass-spectrometry measurement of TCA cycle metabolites and amino acids

GC-MS measurements were performed as described before [11]. Ions used for quantification of metabolite levels were as follows: d5–2HG *m/z* 354; citrate *m/z* 465; alpha-ketoglutarate *m/z* 304; succinate *m/z* 247; fumarate *m/z* 245; malate *m/z* 335; aspartate *m/z* 232; hydroxyproline *m/z* 332; proline *m/z* 216; glutamate *m/z* 246; glutamine *m/z* 245; lactate *m/z* 219; pyruvate *m/z* 174. All peaks were manually inspected and verified relative to known spectra for each metabolite. Peak identification and integration were done with MassHunter software vB.09 (Agilent Technologies). For relative quantification of cell samples, integrated peak areas were normalized to the internal standard d5–2HG and to the packed cell volume of each sample. Absolute quantification of hydroxyproline in tumor acid hydrolysates was performed against a standard curve of commercial *trans*-4-hydroxy-L-proline (Sigma). In stable isotope tracing experiments, natural isotope abundance correction was performed with IsoCor software v1.2. LC-MS measurements were performed as described before [11]. Peak identification and integration were done based on exact mass and retention time match to commercial standards. Data analysis and natural isotope abundance correction were performed with MassHunter Profinder software v10.0 (Agilent Technologies).

Mouse experiments

All animal experiments described adhered to policies and practices approved by Memorial Sloan Kettering Cancer Center's Institutional Animal Care and Use Committee (IACUC)

and were conducted as per NIH guidelines for animal welfare (Protocol Number 11–03-007, Animal Welfare Assurance Number FW00004998). The maximal tumor size/burden permitted by the IACUC (Tumor burden may not exceed 10% of the weight of the mouse which is equivalent to a tumor volume of 2.5 cm^3 for a 25 g mouse) was not exceeded. Mice were maintained under specific pathogen-free conditions and housed at 4–5 mice per cage at a 12-hour light/dark cycle at a relative humidity of 30% to 70% and room temperature of 22.2 ± 1.1°C, and were allowed access to food and water *ad libitum*. Mice were maintained in individually ventilated polysulfone cages with a stainless-steel wire bar lid and filter top on autoclaved aspen chip bedding. Mice were fed a closed-formula, natural-ingredient, γ-irradiated diet (5053 - PicoLab® Rodent Diet 20, Purina LabDiet) which was surface decontaminated using “flash” sterilization (100°C for 1 minute). Mice were provided reverse-osmosis acidified (pH 2.5 to 2.8, with hydrochloric acid) water. Cage bottoms were changed weekly, whereas the wire bar lid, filter top and water bottle were changed biweekly.

Tumor allograft experiments

For the PDAC allograft model in immunocompromised mice, 1×10^5 KPC cells alone or together with 5×10^5 PSCs were resuspended in 100 μL PBS and injected subcutaneously into the flanks of 8–10 weeks old female athymic Nude-Foxn1^{nu} mice (Envigo, 069). For the PDAC allograft model in immunocompetent mice, 5×10^5 KPC cells alone or together with 5×10^5 PSCs were resuspended in 100 μL PBS and injected subcutaneously into the flanks of 8–10 weeks old female syngeneic C57BL/6 mice (JAX, 000664). For the BRCA allograft model, 5×10^5 DB7 cells alone or together with 5×10^5 MFBs were resuspended in 100 μL PBS and injected subcutaneously into the flanks of 8–10 weeks old female syngeneic FVB/N mice (JAX, 001800). In one experiment, we also injected 5×10^5 DB7 cells in 1:1 of 100 μL Matrigel (Corning) and PBS. At the beginning of each experiment, mice were randomly assigned to the different groups. No estimation of sample size was performed before the experiments. Mice were monitored daily, and tumor volume was measured by calipers. Measurements were carried out blindly by members of the MSKCC Antitumor Assessment Core and were taken in two dimensions, and tumor volume was calculated as length x $width^2$ x π/6. At the end of the experiment, mice were euthanized with CO_2, and tumors were collected and aliquoted for 10% formalin fixation and/or snap freezing.

Histology

Tissues were fixed overnight in 10% formalin, dehydrated in ethanol, embedded in paraffin, and cut into 5 μm sections. Picrosirius Red staining was performed with the Picro Sirius Red Stain Kit (Abcam) according to the manufacturer’s instructions. Masson’s trichrome staining was performed with the Masson’s Trichrome Stain Kit (Polysciences) according to the manufacturer’s instructions. For immunofluorescence staining, sections were de-paraffinized with Histo-Clear II (National Diagnostics) and rehydrated according to the manufacturer’s instructions. Antigen retrieval was performed for 40 min in citrate buffer pH 6.0 (Vector Laboratories) in a steamer (IHC World). Sections were blocked in 5% BSA and 5% normal goat serum (Cell Signaling) in TBS containing 0.1% Tween-20, and incubated in primary antibodies at 4°C in a humidified chamber overnight. Sections were incubated in secondary antibody in blocking solution for 1h at room temperature and mounted in Vectashield

Vibrance Antifade Mounting Medium with DAPI (Vector Laboratories). The following primary antibodies were used: SMA (1:400; Millipore, CBL171), CK8 (1:200; DSHB, TROMA-I). The following secondary antibodies were used: donkey anti-mouse Alexa-Fluor 488, donkey anti-rat Alexa Fluor 647 (1:1,000; Thermo Scientific).

Image acquisition and analysis

Images were acquired with a Mirax Slide Scanner at 20x (brightfield) or 40x (immunofluorescence) magnification. For analyses of tumor fibrosis, color deconvolution was performed in Fiji, and the blue channel (Masson's Trichrome) or red channel (Picrosirius Red) were used for quantification. The threshold was determined manually (Picrosirius Red) or with the Yen method (Masson Trichrome) in Fiji. The thresholded (stained) area was quantified as percentage of the total tumor area. Necrotic areas and tumor edges containing skin were identified on H&E-stained consecutive sections and excluded from the analysis. Fibroblasts in tumors were analyzed based on SMA staining in Fiji by subtracting background staining, and thresholding with the Otsu method. The thresholded (stained) area was quantified as percentage of the total tumor area using the same regions as for fibrosis quantification.

Quantification of gene expression

Total RNA was isolated from fibroblasts with Trizol (Life Technologies) according to the manufacturer's instructions, and 1 μg RNA was used for cDNA synthesis using iScript (Bio-Rad). Quantitative real-time PCR (qPCR) analysis was performed in technical triplicates using 1:40 diluted cDNAs and 0.1 μM forward and reverse primers together with Power SYBR Green (Life Technologies) in a QuantStudio 7 Flex (Applied Biosystems). Gene expression was quantified in Microsoft Excel 365 as relative expression ratio using primer efficiencies calculated by a relative standard curve. The geometric mean of the endogenous control genes *18s*, *Actb* and *Rplp0* was used as reference sample. Primer pairs used for qPCR analysis are listed in Supplementary Table 1.

RNA sequencing

Total RNA was isolated with Trizol as above, and libraries were prepared from polyA-selected mRNA using the TruSeq RNAsample preparation kit v2 (Illumina) according to the manufacturer's instructions. Libraries were sequenced using an Illumina HiSeq 4000 generating 150 bp paired-end reads. An average of 65 million reads per sample was retrieved. Adaptor sequences were removed from fastq files with Trimmomatic v.0.36, and trimmed reads were mapped to the mus musculus GRCm38 reference genome using the STAR aligner v.2.5.2b. Aligned features were counted with featureCounts from the Subread package v.1.5.2 and differential expression was determined using DESeq2 v3.10 from Bioconductor in R v4.1.0.

Gene set enrichment analysis (GSEA)

GSEA was performed using a pre-ranked gene list based on the log2 fold change comparing two Ctrl sg samples against a total of four *PC*-ko samples including *PC* sg2 (two samples)

and *PC* sg5 (two samples). GSEA 4.1.0 (Broad Institute) was used with 1000 permutations and mouse gene symbols remapped to human orthologs v7.2 (MSigDB).

tRNA charging assay

Charging status of the indicated tRNA isodecoders was measured as previously described [20]. In brief, Trizol-chloroform extracts were precipitated with 2.7x volumes of cold ethanol in presence of 30 μg GlycoBlue (ThermoFisher) overnight. Samples were resuspended in 0.3 M acetate buffer (pH 4.5) with 10 mM EDTA and precipitated overnight. Samples were resuspended in 10 mM acetate buffer with 1 mM EDTA. 2 μg of each RNA sample was treated with 10 mM of either sodium periodate (Sigma) ('oxidized sample') or sodium chloride ('non-oxidized sample') and incubated for 20 min at room temperature in the dark. Reactions were quenched with glucose for 15 min. Yeast Phe-tRNA (Sigma) was spiked into each sample, followed by ethanol precipitation. Samples were resuspended in 50 mM Tris buffer (pH 9) and incubated for 50 min at 37°C, quenched with acetate buffer and precipitated. Samples were resuspended in RNAse-free water and ligated to a 5' adenylated DNA adaptor using truncated KQ mutant T4 RNA ligase 2 (New England Biolabs) for 3h at room temperature. Reverse transcription was performed with SuperScript IV reverse transcriptase (Thermo Scientific) according to the manufacturer's instructions, with a primer complementary to the DNA adaptor. cDNA samples were subjected to qPCR with tRNA isodecoder-specific primer pairs listed in Supplementary Table 1. Ct values obtained with primers specific for yeast Phe-tRNA were subtracted from Ct values obtained with isodecoder-specific primers. The charged fraction was calculated based on the relative difference between the delta-Ct value of a non-oxidized (representing total) and oxidized (representing charged) sample for each primer pair.

Chromatin Immunoprecipitation (ChIP)

Cells were crosslinked in 1% formaldehyde (Thermo Scientific) in PBS for 10 min at room temperature. After quenching with 2.5 M glycine, cell pellets were collected and stored at −80°C until further processing. One replicate per sample was collected at a time. After all replicates were collected, cells were lysed and subjected to chromatin shearing with the Covaris sonicator (E220) for 25 min. The supernatant was cleared and diluted in the same sonication buffer but without N-lauroylsarcosine. 500 μg extract was subjected to immunoprecipitation with 1 μg H3K27me3 (Cell Signaling, 9733S) or 2 μg H3K27ac (Active Motif, 39034) antibody or an equivalent amount of IgG control (Santa Cruz, sc-66931 or sc-69786) using Protein G magnetic beads (Thermo Scientific) at 4°C overnight. The beads were washed, and DNA was reverse-crosslinked overnight and purified using a PCR purification kit (QIAGEN). ChIPed DNA was quantified by qPCR in technical triplicates using 1:10 diluted cDNAs and 0.1 μM forward and reverse primers together with Power SYBR Green (Life Technologies) in a QuantStudio 7 Flex (Applied Biosystems). Primer pairs used for ChIP-qPCR analysis are listed in Supplementary Table 1. Enrichment was calculated in Microsoft Excel 365 as percent of input control using a relative standard curve for each primer pair.

DNA motif analysis

Human SMAD2/3/4 motif position frequency matrices were downloaded from the JASPAR database (2020, 8th release). A sequence spanning the putative promoter regions and transcriptional start site (TSS) of three different human PC isoforms was downloaded from the UCSC genome browser (hg38_dna range=chr11:66847159–66962459). Motif searching was performed using FIMO from the MEME Suite with a cutoff of $P<0.0001$.

Statistics

A student's *t*-test was applied to compare one variable between two groups. One-way ANOVA was applied to compare one variable between three or more groups. Two-way ANOVA was applied to compare two independent variables between two groups. Correction for multiple comparisons was done using the Holm-Sidak method. Pearson correlation was applied to analyze correlation between data from two groups. Statistical analysis was done in GraphPad Prism 8. Most graphs show the mean + SD with individual datapoints, unless indicated otherwise in the figure legends.

Extended Data

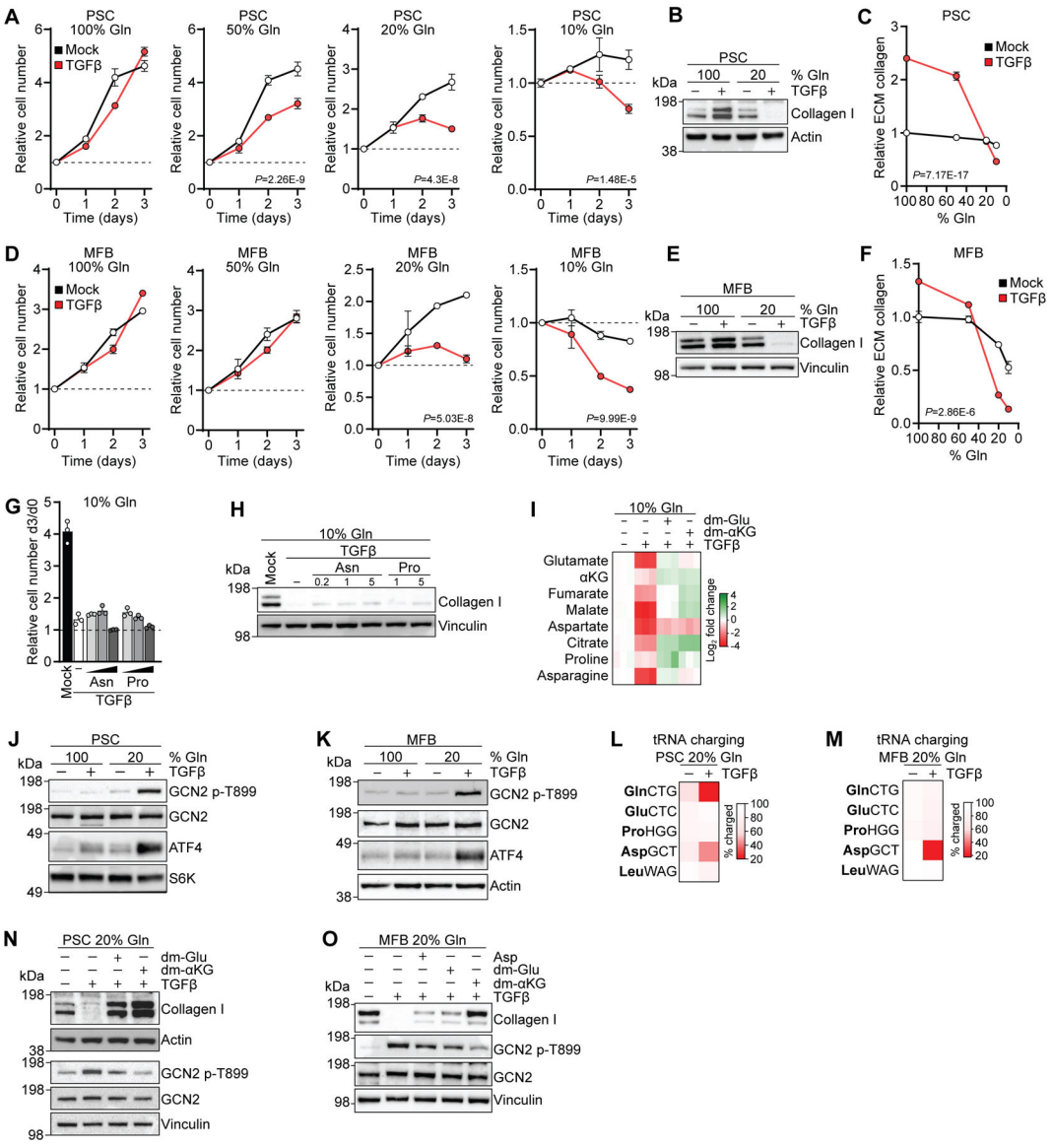

Extended Data Fig. 1. TGFβ-induced collagen synthesis is linked to glutamine-dependent TCA cycle anaplerosis

(A) Growth curves of PSCs cultured in the indicated percentage of Gln and treated with TGFβ (2 ng/mL). n=3 biologically independent samples. (B) Western Blot of PSCs cultured in 100% or 20% Gln and treated with TGFβ for 48h. (C) Collagen abundance in ECM derived from confluent PSCs cultured in the indicated percentage of Gln and treated with TGFβ. n=3 biologically independent samples. (D) Growth curves of MFBs cultured in the indicated percentage of Gln and treated with TGFβ. n=3 biologically independent samples. (E) Western Blot of MFBs cultured in 100% or 20% Gln and treated with TGFβ for 48h. (F) Collagen abundance in ECM derived from confluent MFBs cultured in the indicated percentage of Gln and treated with TGFβ. n=3 biologically independent samples. (G) Relative number of NIH-3T3 cells cultured in 10% Gln and treated with TGFβ and 0.2,

1 or 5 mM of asparagine (Asn) or proline (Pro). n=3 biologically independent samples. (H) Western Blot of NIH-3T3 cells cultured in 10% Gln and treated with TGFβ and the indicated metabolites and concentrations for 48h. (I) Relative metabolite abundance in NIH-3T3 cells cultured in 10% Gln and treated with TGFβ and dm-Glu (5 mM) or dm-αKG (5 mM) for 48h. n=3 biologically independent samples. (J,K) Western Blot of PSCs (J) or MFBs (K) cultured in 100% or 20% Gln and treated with TGFβ for 48h. (L,M) tRNA charging in PSCs (L) or MFBs (M) cultured in 20% Gln and treated with TGFβ for 48h. n=1 independent experiment. (N,O) Western Blot of PSCs (N) or MFBs (O) cultured in 20% Gln and treated with TGFβ and dm-Glu or dm-αKG for 48h. MFBs were also treated with aspartate (Asp, 20 mM).

Mean±SD (A,C,D,F) or mean+SD (G) are shown. Dashed lines (A,D,G) represent cell number at day 0. Two-way ANOVA (A,C,D,F). Western blots are representative of three (B,E,J,K) or two (H,N,O) independent experiments. tRNA charging analyses (L,M) are representative of two independent experiments. All other experiments were performed at least twice.

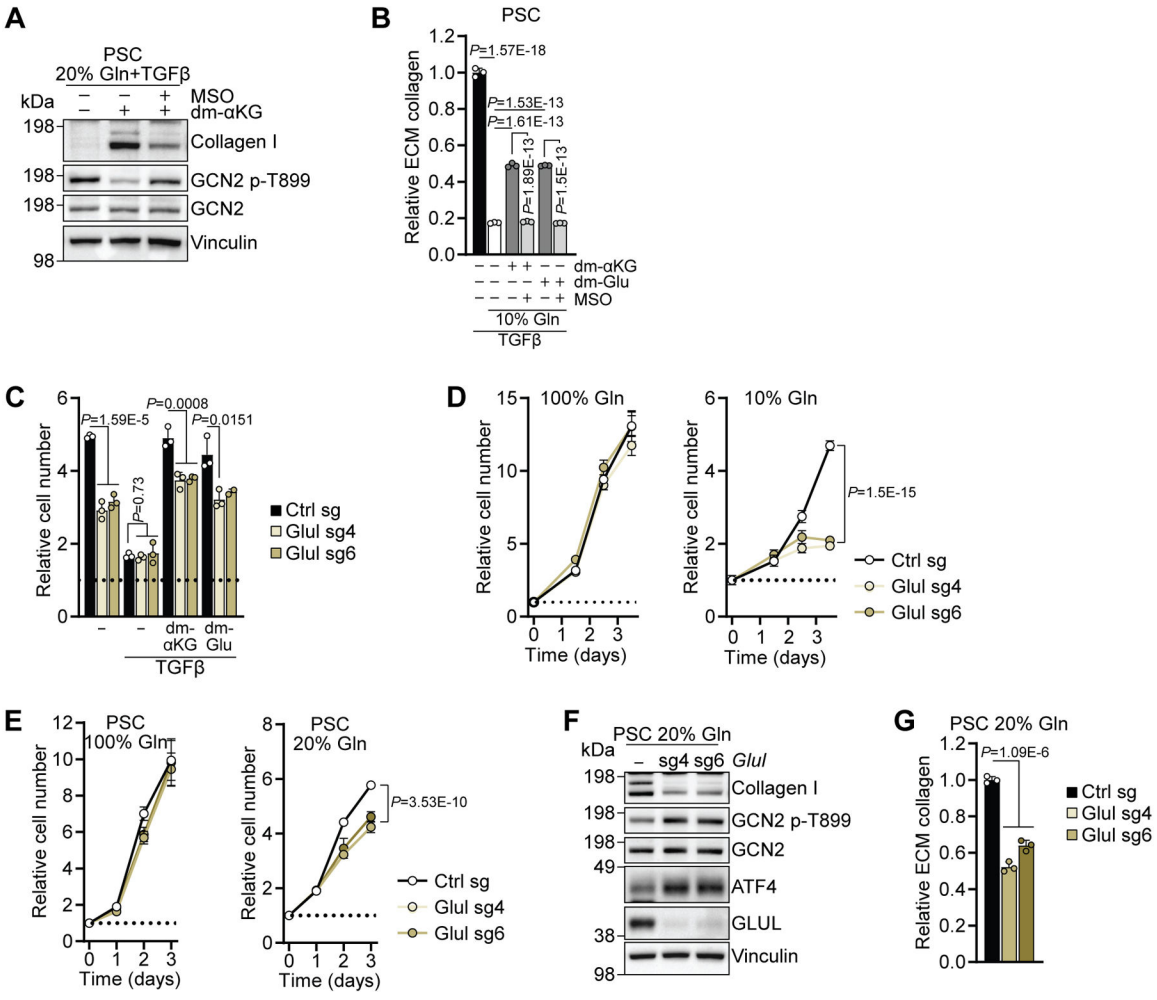

Extended Data Fig. 2. Glutamine de novo synthesis can maintain collagen synthesis and proliferation when glutamine is limiting

(A) Western Blot of PSCs cultured in 20% Gln in the presence of TGFβ and treated with dm-αKG and MSO. (B) Collagen abundance of in ECM derived from confluent PSCs cultured in 100% or 10% Gln in the presence of TGFβ and treated with dm-αKG, dm-Glu and MSO. n=3 biologically independent samples. (C) Relative number of NIH-3T3 cells expressing Ctrl or Glul sgRNA, cultured in 10% Gln and treated with TGFβ alone and dm-αKG or dm-Glu. n=2 (Glul-sg6 dm-Glu), n=3 (all others) biologically independent samples. (D,E) Growth curves of NIH-3T3 cells (D) or PSCs (E) expressing Ctrl or Glul sgRNA, cultured in 100% or 10% Gln/20% Gln. n=3 biologically independent samples. (F) Western Blot of PSCs expressing Ctrl or Glul sgRNA, cultured in 20% Gln for 48h. (G) Collagen abundance in ECM derived from confluent PSCs expressing Ctrl or Glul sgRNA, cultured in 20% Gln. n=3 biologically independent samples.

Mean+SD (B,C,G) or mean±SD (D,E) are shown. One-way ANOVA with Holm-Sidak correction (B), one-way ANOVA (C,G), two-sided unpaired t-test (C: Glul-sg6 dm-Glu), two-way ANOVA (D,E). Western blots (A,F) are representative of three independent experiments. All other experiments were performed at least twice.

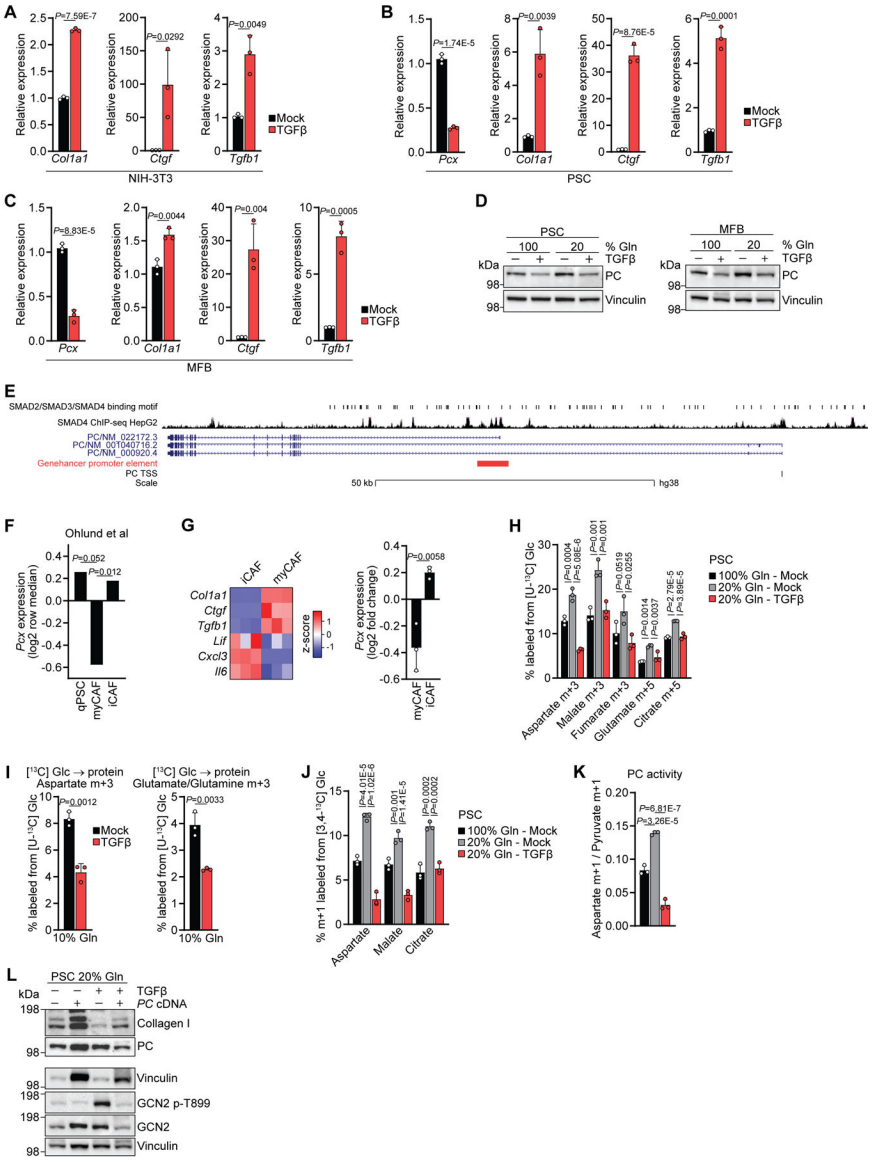

Extended Data Fig. 3. TGFβ suppresses PC expression and reduces PC activity

(A-C) mRNA expression of the indicated genes in NIH-3T3 cells (A), PSCs (B) or MFBs (C) cultured in 100% Gln and treated with TGFβ for 24h. n=3 biologically independent samples. (D) Western Blot of PSCs (left) or MFBs (right) cultured in 100% or 20% Gln and treated with TGFβ for 48h. (E) UCSC genome browser tracks showing putative SMAD2/SMAD3/SMAD4 binding motifs, SMAD4 ChIP-seq peaks in HepG2 cells, the Genehancer promoter element and the PC transcriptional start site (TSS) at the genomic loci of three human PC isoforms. (F) Pcx expression from RNA-sequencing of quiescent PSCs (qPSC), myofibroblastic CAFs (myCAF) and inflammatory CAFs (iCAFs). Data and p-values are from GSE93313. (G) mRNA expression of myCAF and iCAF markers in iCAFs and myCAFs (left); Pcx mRNA expression in myCAFs and iCAFs, relative to qPSCs (right). n=3 biologically independent samples. (H) [U-13C]-Glc tracing in PSCs cultured in 100% or 20% Gln and treated with TGFβ for 48h. n=3 biologically independent samples. (I)

[U-13C]-Glc tracing into indicated amino acid residues of cellular proteins. NIH-3T3 cells were cultured in 10% Gln and treated with TGFβ for 48h. n=3 biologically independent samples. (J,K) [3,4–13C]-Glc tracing in PSCs cultured in 100% or 20% Gln and treated with TGFβ for 48h. M+1 labeling (J). PC activity (K). n=3 biologically independent samples. (L) Western Blot of PSCs expressing empty vector or human PC cDNA, cultured in 20% Gln and treated with TGFβ.

Mean+SD (A-C,G-K) are shown. Two-sided unpaired t-test (A-C,G,I), by one-way ANOVA with Holm-Sidak correction (H,J,K). Western blots (D,L) are representative of two independent experiments. (3,4–13C)-Glc tracing in PC-ko cells (F) was performed once. All other experiments were performed at least twice.

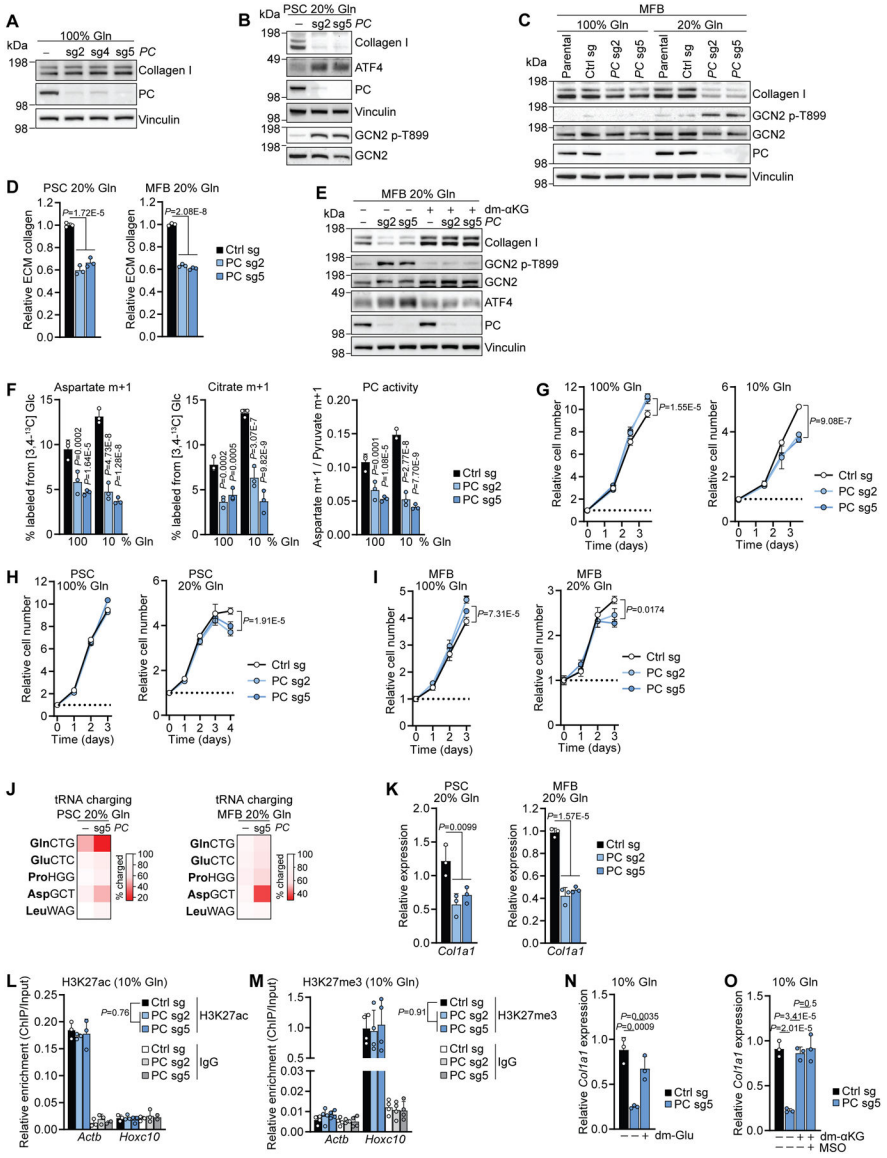

Extended Data Fig. 4. PC is required for collagen synthesis when extracellular glutamine is low

(A) Western Blot of NIH-3T3 cells expressing Ctrl or PC sgRNA, cultured in 100% Gln for 48h. (B) Western Blot of PSCs expressing Ctrl or PC sgRNA, cultured in 20% Gln for 48h.

(C) Western Blot of parental MFBs and MFBs expressing Ctrl or PC sgRNA, cultured in 100% or 20% Gln for 48h. (D) Collagen abundance in ECM derived from confluent PSCs (left) or MFBs (right) expressing Ctrl or PC sgRNA, cultured in 20% Gln. n=3 biologically independent samples. (E) Western Blot of MFBs expressing Ctrl or PC sgRNA, cultured in 20% Gln and treated with dm-αKG for 48h. (F) [3,4–13C]-Glc tracing in NIH-3T3 cells expressing Ctrl or PC sgRNA cultured in 100% or 10% Gln for 48h. n=3 biologically independent samples. (G-I) Growth curves of NIH-3T3 cells (G), PSCs (H) or MFBs (I) expressing Ctrl or PC sgRNA, cultured in 100% or 10%/20% Gln. n=3 biologically independent samples. (J) tRNA charging in PSCs (left) or MFBs (right) expressing Ctrl or PC sgRNA, cultured in 20% Gln for 48h. n=1 independent experiment. (K) Col1a1 mRNA expression in PSCs (left) or MFBs (right) expressing Ctrl or PC sgRNA, cultured in 20% Gln for 48h. n=3 biologically independent samples. (L,M) H3K27ac (L) or H3K27me3 enrichment (M) in NIH-3T3 cells expressing Ctrl or PC sgRNA, cultured in 10% Gln for 48h. n=3 (L), n=4 (M) independent experiments. (N,O) Col1a1 mRNA expression in NIH-3T3 cells expressing Ctrl or PC sgRNA, cultured in 10% Gln for 48h. Cells were treated with dm-Glu (N) or dm-αKG and MSO (O). n=3 biologically independent samples. Mean±SD (G-I), mean+SD (D, F, K-O) are shown. Dashed lines (G-I) represent cell number at day 0. Two-way ANOVA (F-I), one-way ANOVA (D,K), two-way ANOVA (L,M) analyzing the effects of PC-ko on H3K27ac or H3K27me3 across the analyzed genomic regions, one-way ANOVA with Holm-Sidak correction (N,O). Western blots are representative of two (A,E) or three (B,C) independent experiments. tRNA charging analysis (J) is representative of two independent experiments. All other experiments were performed at least twice.

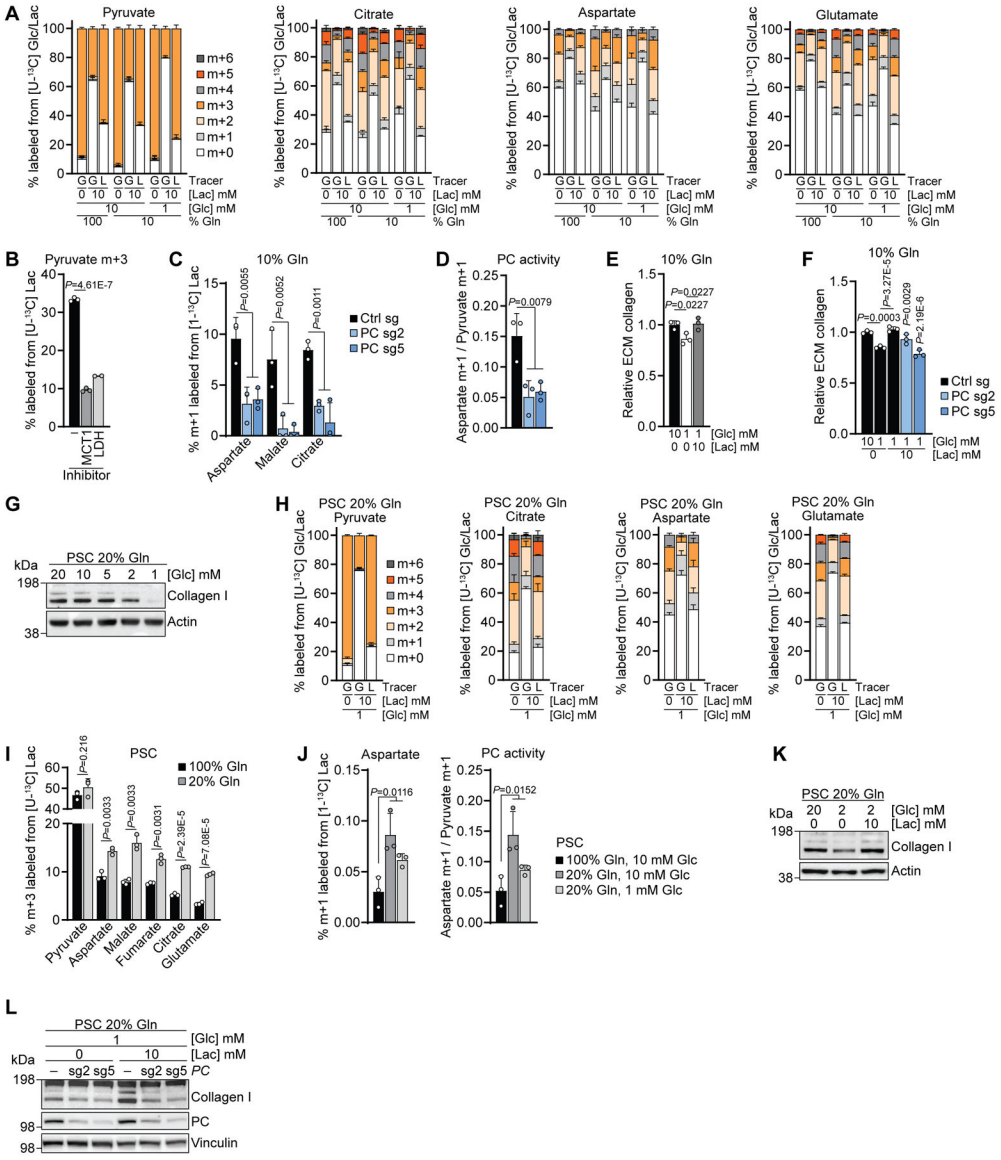

Extended Data Fig. 5. Fibroblasts take up and use lactate for TCA cycle anaplerosis via PC

(A) [U-13C]-Glc and [U-13C]-Lac tracing. NIH-3T3 cells were cultured for 48h in 100% or 10% Gln in the presence of 10 or 1 mM D-glucose with or without 10 mM Na-lactate. M+3 isotopologues are shown in Fig. 6B. G, glucose; L, lactate. n=3 biologically independent samples. (B) [U-13C]-Lac tracing. NIH-3T3 cells were cultured in 10% Gln and treated with AZD3965 (MCT1 inhibitor, 5 μM) or sodium oxamate (LDH inhibitor, 10 mM) for 8h. [U-13C]-Lac was added in the last 1h. n=2 (LDHi), n=3 (all others) biologically independent samples. (C,D) [1–13C]-Lac tracing in NIH-3T3 cells expressing Ctrl or PC sgRNA cultured in 10% Gln in the presence of 10 mM Na-lactate for 48h. M+1 labeling (C). PC activity (D). n=3 biologically independent samples. (E,F) Collagen abundance in ECM generated by confluent parental (E) or Ctrl or PC sgRNA expressing NIH-3T3 cells (F) cultured in 10% Gln and the indicated concentrations of D-glucose and Na-lactate. n=3 biologically independent samples. (G) Western Blot of PSCs cultured in 20% Gln and the

indicated concentrations of D-glucose for 48h. (H) [U-13C]-Glc and [U-13C]-Lac tracing into indicated metabolites. PSCs were cultured for 48h in 20% Gln and 1 mM D-glucose with or without 10 mM Na-lactate. n=3 biologically independent samples. (I) [U-13C]-Lac tracing in PSCs cultured in 100% or 20% Gln for 48h. n=3 biologically independent samples. (J) [1–13C]-Lac tracing. PSCs were cultured for 48h in 100% or 20% Gln in the presence of 10 or 1 mM D-glucose and 10 mM Na-lactate. n=3 biologically independent samples. (K) Western Blot of PSCs cultured in 20% Gln and the indicated concentrations of D-glucose and Na-lactate for 48h. (L) Western Blot of PSCs expressing Ctrl or PC sgRNA, cultured in 20% Gln and the indicated concentrations of D-glucose and Na-lactate for 48h. Mean+SD (A-F,H-J) are shown. Two-sided unpaired t-test (B), one-way ANOVA (C,D,J), one-way ANOVA with Holm-Sidak correction (E,F), two-sided unpaired t-test with Holm-Sidak correction (I). Western blots (G,K,L) are representative of two independent experiments. [U-13C]-Lac tracing in PSC in low glucose (H) was performed once. All other experiments were performed at least twice.

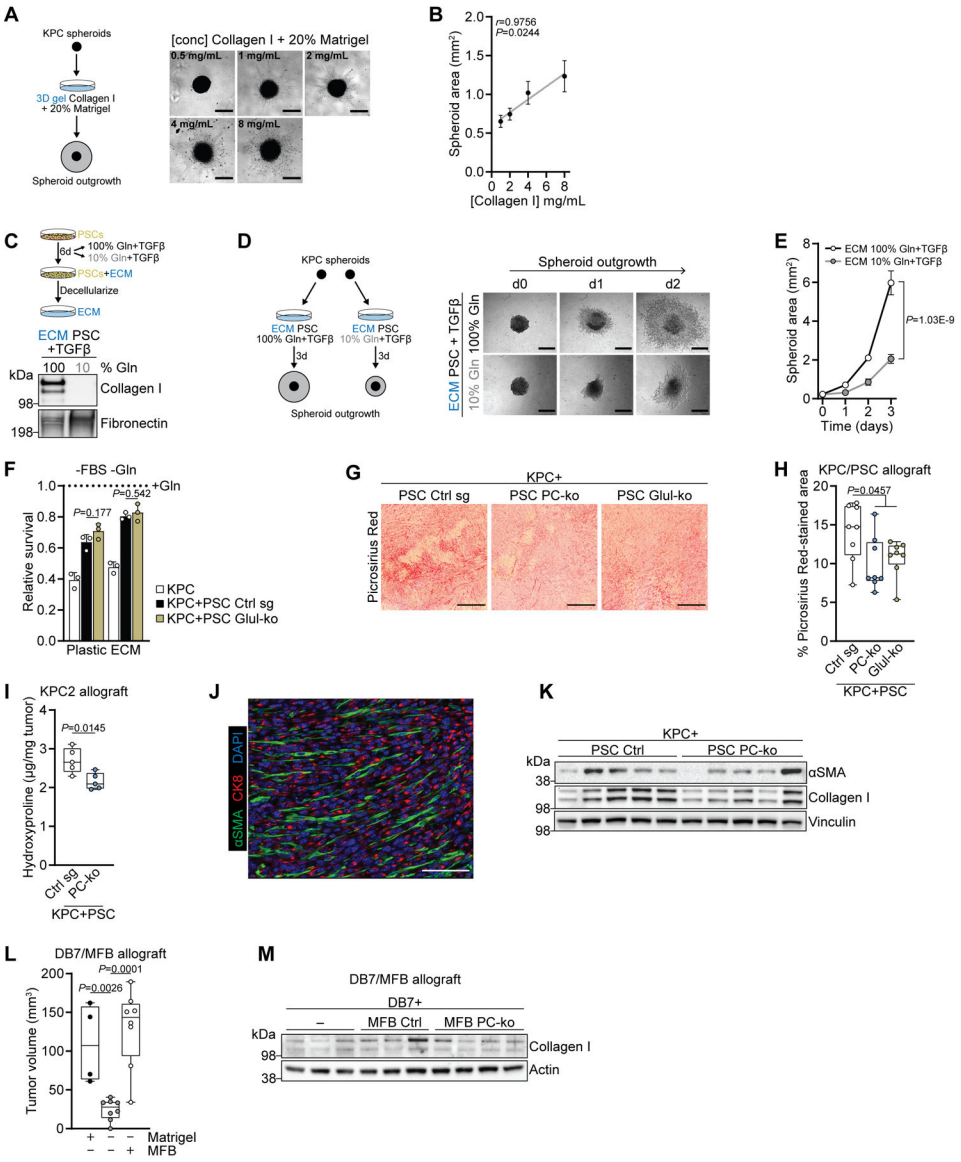

Extended Data Fig. 6. Fibroblast PC supports tumor fibrosis and growth

(A) Outgrowth of KPC spheroids on top of a synthetic ECM (3D gel) Representative images are shown. Scale bar=500 µm. (B) Pearson correlation of total spheroid area from (A) with collagen I concentration used to prepare the synthetic ECM. n=4 biologically independent samples. (C,D) Western blot of ECM generated by confluent PSCs cultured in 100% or 10% Gln in the presence of TGFβ (C). (D) Outgrowth of KPC spheroids on top of this ECM. Representative images are shown. Scale bar=500 µm. (E) Quantification of spheroid outgrowth from (D). n=8 biologically independent samples. (F) Survival of KPC-GFP cells after 3 days co-culture with Ctrl or Glul sgRNA expressing PSCs on plastic or PSC-derived ECM in the absence of FBS and Gln. n=3 biologically independent samples. (G-K) KPC/PSC allograft experiment in nude mice. (G) Representative images of Picrosirius staining of KPC/PSC allografts at day 25 after injection. Scale bar=500 µm. (H) Quantification of Picrosirius staining of KPC/PSC allografts. n=8 biologically independent

tumors. (I) Collagen levels in KPC/PSC allografts at day 25 after injection. n=5 biologically independent tumors. (J) Representative image of KPC/PSC allograft tumors stained for αSMA, CK8 and DAPI. Scale bar=100 μm. (K) Western Blot of KPC/PSC allografts at day 25 after injection. (L) Volume of DB7 allografts 8 days after injection of DB7 cells alone, with Matrigel or with MFBs. n=4 (DB7+Matrigel), n=8 (DB7, DB7+MFB) biologically independent tumors. (M) Western Blot of the second batch of DB7/MFB allografts 8 days after injection. The first batch is shown in Fig. 7L.

Mean±SD (B,E), median with 25% to 75% percentile box and min/max whiskers (H,I,L), mean+SD (F) are shown. Pearson correlation followed by two-sided unpaired t-test (B), two-way ANOVA (E), two-way ANOVA with Holm-Sidak correction (F), one-way ANOVA (H), two-sided unpaired t-test (I), one-way ANOVA with Holm-Sidak correction (L). Western blots were performed once with 5 (K) or 3–4 (M) biologically independent tumors, or were performed twice (C). Spheroid experiments were performed twice. Tumor growth, staining and hydroxyproline experiments were performed once with multiple biologically independent tumors.

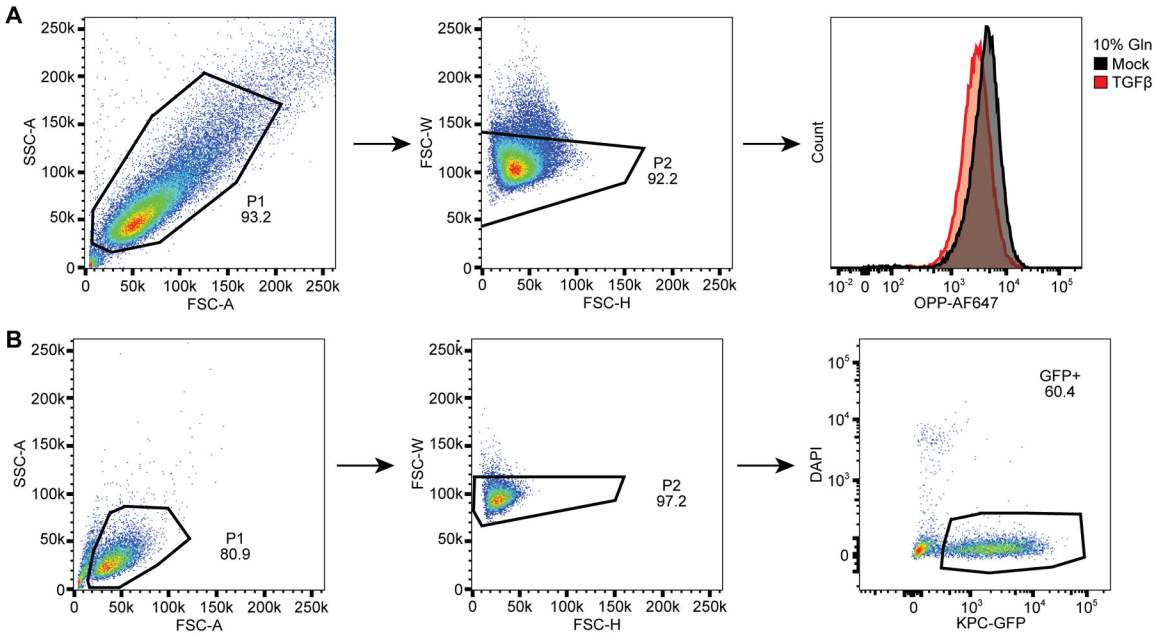

Extended Data Fig. 7. Gating strategy for flow cytometry

(A) Gating strategy for OPP staining. Data are from Figure 1F. (B) Gating strategy for KPC-GFP and PSC co-culture assay. Data are from Extended Data Figure 6F.

Supplementary Material

Refer to Web version on PubMed Central for supplementary material.

Acknowledgments

We thank the reviewers for their contribution to the external peer review of our manuscript. We thank the members of the Thompson laboratory for helpful discussions. We are thankful to Tullia Lindsten for help with planning of and protocol preparation for mouse experiments, and to Jiajun Zhu for help with optimization of ChIP experiments. We also thank Elisa De Stanchina and Omar Hayatt from the MSKCC Antitumor Assessment Core for help with

tumor allograft experiments. S.S. was supported by postdoctoral fellowships from the Human Frontier Science Program (LT000854/2018) and the European Molecular Biology Organization (ALTF 467–2018). S.S. also received support from the NCI (1K99CA259224) and the Alan and Sandra Gerry Metastasis and Tumor Ecosystems Center. X.C. was supported by the NCI (1K99CA256505). G.M.S. was supported by the NCI (K22CA218472) and the Herbert and Maxine Block Memorial Lectureship Fund. C.B.T. was supported by the NCI (R01CA201318). This work was also supported by the cancer center support grant (P30CA008748) to MSKCC.

Data availability

RNA-sequencing data that support the findings of this study have been deposited into the NCBI Gene Expression Omnibus (GEO) with the accession code GSE169588. Human SMAD2/3/4 motif position frequency matrices can be found on JASPAR with the accession code MA0513.1. USCS genome browser tracks are accessible via the following link: http://genome.ucsc.edu/cgi-bin/hgTracks?db=hg38&lastVirtModeType=default&lastVirtModeExtraState=&virtModeType=default&virtMode=0&nonVirtPosition=&position=chr11%3A66847371%2D66973751&hgsid=1152675631_ClzjvmWXzEUYlG9AcUArh1LlTkiY. Additional information can be found in the Nature Research Reporting Summary. Further information and requests for reagents may be directed to, and will be fulfilled by, the corresponding author. Source data are provided with this paper. All data supporting the findings of this study are available from the corresponding author on reasonable request.

References

1. Kalluri R The biology and function of fibroblasts in cancer. Nat. Rev. Cancer 16, 582–598 (2016). [PubMed: 27550820]
2. Hanahan D & Weinberg RA The hallmarks of cancer. Cell 100, 57–70 (2000). [PubMed: 10647931]
3. Dvorak HF Tumors: wounds that do not heal. Similarities between tumor stroma generation and wound healing. N. Engl. J. Med 315, 1650–9 (1986). [PubMed: 3537791]
4. Winslow S, Lindquist KE, Edsjö A & Larsson C The expression pattern of matrix-producing tumor stroma is of prognostic importance in breast cancer. BMC Cancer 16, 1–13 (2016).
5. Lim S. Bin, Tan SJ, Lim WT & Lim CT An extracellular matrix-related prognostic and predictive indicator for early-stage non-small cell lung cancer. Nat. Commun 8, 1–10 (2017). [PubMed: 28232747]
6. Whatcott CJ et al. Desmoplasia in primary tumors and metastatic lesions of pancreatic cancer. Clin. Cancer Res 21, 3561–3568 (2015). [PubMed: 25695692]
7. Pickup MW, Mouw JK & Weaver VM The extracellular matrix modulates the hallmarks of cancer. EMBO Rep 15, 1243–1253 (2014). [PubMed: 25381661]
8. Provenzano PP et al. Collagen density promotes mammary tumor initiation and progression. BMC Med 6, 1–15 (2008). [PubMed: 18234075]
9. Hamanaka RB & Mutlu GM Metabolic requirements of pulmonary fibrosis: role of fibroblast metabolism. FEBS J 1–22 (2021)
10. Nigdelioglu R et al. Transforming Growth Factor (TGF)-β Promotes de Novo Serine Synthesis for Collagen Production. J. Biol. Chem 291, 27239–27251 (2016). [PubMed: 27836973]
11. Schwörer S et al. Proline biosynthesis is a vent for TGFβ-induced mitochondrial redox stress. EMBO J 39, e103334 (2020). [PubMed: 32134147]
12. Psychogios N et al. The human serum metabolome. PLoS One 6, (2011).
13. Schwörer S, Vardhana SA & Thompson CB Cancer Metabolism Drives a Stromal Regenerative Response. Cell Metab 29, 576–591 (2019). [PubMed: 30773467]
14. Fläring UB, Rooyackers OE, Wernerman J & Hammarqvist F Glutamine attenuates post-traumatic glutathione depletion in human muscle. Clin. Sci 104, 275–282 (2003).

15. Kamphorst JJ et al. Human pancreatic cancer tumors are nutrient poor and tumor cells actively scavenge extracellular protein. Cancer Res 75, 544–553 (2015). [PubMed: 25644265]
16. Pan M et al. Regional glutamine deficiency in tumours promotes dedifferentiation through inhibition of histone demethylation. Nat. Cell Biol 18, 1090–1101 (2016). [PubMed: 27617932]
17. Ho PC et al. Phosphoenolpyruvate Is a Metabolic Checkpoint of Anti-tumor T Cell Responses. Cell 162, 1217–1228 (2015). [PubMed: 26321681]
18. Avagliano A et al. Influence of Fibroblasts on Mammary Gland Development, Breast Cancer Microenvironment Remodeling, and Cancer Cell Dissemination. Cancers (Basel) 12, 1697 (2020).
19. Hwang RF et al. Cancer-associated stromal fibroblasts promote pancreatic tumor progression. Cancer Res 68, 918–926 (2008). [PubMed: 18245495]
20. Pavlova NN et al. Translation in amino-acid-poor environments is limited by tRNAGln charging. Elife 9, 1–27 (2020).
21. Lu PD, Harding HP & Ron D Translation reinitiation at alternative open reading frames regulates gene expression in an integrated stress response. J. Cell Biol 167, 27–33 (2004). [PubMed: 15479734]
22. Zhu J & Thompson CB Metabolic regulation of cell growth and proliferation. Nat. Rev. Mol. Cell Biol (2019)
23. Yang L et al. Targeting Stromal Glutamine Synthetase in Tumors Disrupts Tumor Microenvironment-Regulated Cancer Cell Growth. Cell Metab 24, 685–700 (2016). [PubMed: 27829138]
24. Francescone R et al. Netrin G1 promotes pancreatic tumorigenesis through cancer associated fibroblast driven nutritional support and immunosuppression. Cancer Discov CD-20–0775 (2020)
25. Cheng T et al. Pyruvate carboxylase is required for glutamine-independent growth of tumor cells. Proc. Natl. Acad. Sci. U. S. A 108, 8674–8679 (2011). [PubMed: 21555572]
26. Sellers K et al. Pyruvate carboxylase is critical for non-small-cell lung cancer proliferation. J. Clin. Invest 125, 687–698 (2015). [PubMed: 25607840]
27. Lau AN et al. Dissecting cell-type-specific metabolism in pancreatic ductal adenocarcinoma. Elife 9, 1–35 (2020).
28. Davidson SM et al. Environment impacts the metabolic dependencies of ras-driven non-small cell lung cancer. Cell Metab 23, 517–528 (2016). [PubMed: 26853747]
29. Öhlund D et al. Distinct populations of inflammatory fibroblasts and myofibroblasts in pancreatic cancer. J. Exp. Med jem.20162024 (2017)
30. Schvartzman JM, Thompson CB & Finley LWS Metabolic regulation of chromatin modifications and gene expression. J. Cell Biol jcb.201803061 (2018)
31. Goveia J et al. Meta-analysis of clinical metabolic profiling studies in cancer: challenges and opportunities. EMBO Mol. Med 8, 1134–1142 (2016). [PubMed: 27601137]
32. Hui S et al. Glucose feeds the TCA cycle via circulating lactate. Nature 551, 115–118 (2017). [PubMed: 29045397]
33. Marin-Valencia I, Roe CR & Pascual JM Pyruvate carboxylase deficiency: Mechanisms, mimics and anaplerosis. Mol. Genet. Metab 101, 9–17 (2010). [PubMed: 20598931]
34. Cappel DA et al. Pyruvate-Carboxylase-Mediated Anaplerosis Promotes Antioxidant Capacity by Sustaining TCA Cycle and Redox Metabolism in Liver. Cell Metab 29, 1291–1305.e8 (2019). [PubMed: 31006591]
35. Groen AK, Roermund van CWT, Vervoorn RC & Tager JM Control of gluconeogenesis in rat liver cells. Biochem. J 237, 379–389 (1986). [PubMed: 3800895]
36. Uzgare A, Sandra K, Zhang Q, Cynober L & Barbul A Ornithine alpha ketoglutarate enhances wound healing. J. Am. Coll. Surg 209, S72 (2009).
37. Cynober L, Lasnier E, Le Boucher J, Jardel A & Coudray-Lucas C Effect of ornithine α-ketoglutarate on glutamine pools in burn injury: Evidence of component interaction. Intensive Care Med 33, 538–541 (2007). [PubMed: 17235510]
38. Williams LM et al. Identifying collagen VI as a target of fibrotic diseases regulated by CREBBP/EP300. Proc. Natl. Acad. Sci. U. S. A 117, 20753–20763 (2020). [PubMed: 32759223]

39. Eckert MA et al. Proteomics reveals NNMT as a master metabolic regulator of cancer-associated fibroblasts. Nature 569, 723–728 (2019). [PubMed: 31043742]
40. Bhagat TD et al. Lactate-mediated epigenetic reprogramming regulates formation of human pancreatic cancer-associated fibroblasts. Elife 8, 1–23 (2019).
41. Chen Y et al. Type I collagen deletion in αSMA+ myofibroblasts augments immune suppression and accelerates progression of pancreatic cancer. Cancer Cell 1–18 (2021) [PubMed: 33434507]
42. Amaral JF, Shearer JD, Mastrofrancesco B, Gann DS & Caldwell MD Can lactate be used as a fuel by wounded tissue? Surgery 100, 252–61 (1986). [PubMed: 3738754]
43. Becker LM et al. Epigenetic Reprogramming of Cancer-Associated Fibroblasts Deregulates Glucose Metabolism and Facilitates Progression of Breast Cancer. Cell Rep 31, 107701 (2020). [PubMed: 32492417]
44. Knudsen ES, Balaji U, Freinkman E, McCue P & Witkiewicz AK Unique metabolic features of pancreatic cancer stroma: relevance to the tumor compartment, prognosis, and invasive potential. Oncotarget 7, 78396–78411 (2016). [PubMed: 27623078]
45. Quek L-E, Liu M, Joshi S & Turner N Fast exchange fluxes around the pyruvate node: a leaky cell model to explain the gain and loss of unlabelled and labelled metabolites in a tracer experiment. Cancer Metab 4, 1–14 (2016).
46. Vaupel P, Kallinowski F & Okunieff P Blood flow, oxygen and nutrient supply, and metabolic microenvironment of human tumors: a review. Cancer Res 49, 6449–65 (1989). [PubMed: 2684393]
47. Olivares O et al. Collagen-derived proline promotes pancreatic ductal adenocarcinoma cell survival under nutrient limited conditions. Nat. Commun 8, 16031 (2017). [PubMed: 28685754]
48. Zhu Z et al. Tumour-reprogrammed stromal BCAT1 fuels branched-chain ketoacid dependency in stromal-rich PDAC tumours. Nat. Metab 2, 775–792 (2020). [PubMed: 32694827]
49. Jesnowski R et al. Immortalization of pancreatic stellate cells as an in vitro model of pancreatic fibrosis: Deactivation is induced by matrigel and N-acetylcysteine. Lab. Investig 85, 1276–1291 (2005). [PubMed: 16127427]
50. Soule HD & McGrath CM A simplified method for passage and long-term growth of human mammary epithelial cells. Vitr. Cell. Dev. Biol 22, 6–12 (1986).

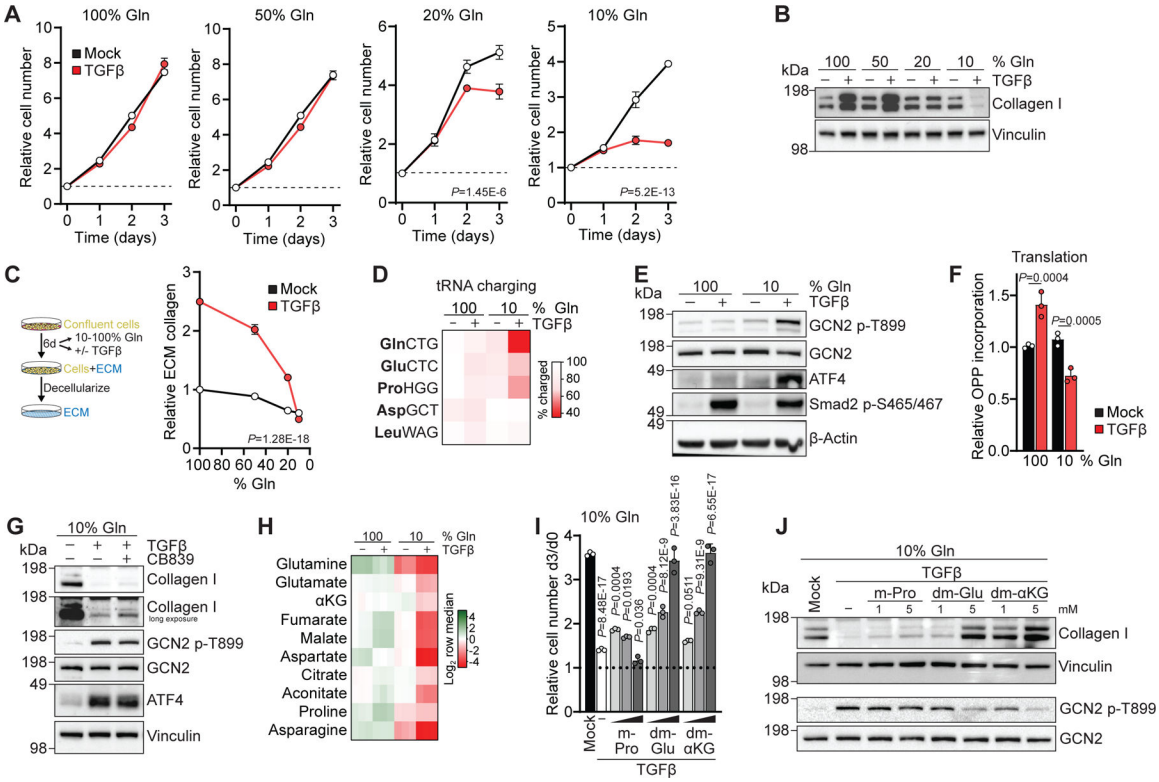

Figure 1: TGFβ-induced collagen synthesis is linked to glutamine dependent TCA cycle anaplerosis.

(A) Growth curves of NIH-3T3 cells cultured in the indicated percentage of Gln and treated with TGFβ (2 ng/mL). *n*=3 biologically independent samples. Dashed line indicates cell number at d0. **(B)** Western Blot of NIH-3T3 cells cultured in the indicated percentage of Gln and treated with TGFβ for 48h. **(C)** Schematic of fibroblast-derived ECM preparation (left); collagen abundance in ECM derived from confluent NIH-3T3 cells cultured in the indicated percentage of Gln and treated with TGFβ (right). *n*=3 biologically independent samples. **(D)** tRNA charging in NIH-3T3 cells cultured in 100% or 10% Gln and treated with TGFβ for 48h. *n*=1 independent experiment. **(E)** Western Blot of NIH-3T3 cells cultured in 100% or 10% Gln and treated with TGFβ for 48h. **(F)** Relative translation rate of NIH-3T3 cells cultured in 100% or 10% Gln and treated with TGFβ for 48h. *n*=3 biologically independent samples. **(G)** Western Blot of NIH-3T3 cells cultured in 10% Gln and treated with TGFβ and CB839 (1 μM) for 48h. **(H)** Relative metabolite abundance in NIH-3T3 cells cultured in 100% or 10% Gln and treated with TGFβ for 48h. *n*=3 biologically independent samples. **(I)** Relative number of NIH-3T3 cells cultured in 10% Gln and treated with TGFβ and 0.2, 1 or 5 mM of the indicated cell-permeable metabolites for 3 days. m-Pro, L-proline-methylester; dm-Glu, L-glutamic acid dimethylester; dm-αKG, Dimethyl alpha-ketoglutarate. *n*=3 biologically independent samples. **(J)** Western Blot of NIH-3T3 cells cultured in 10% Gln and treated with TGFβ and the indicated concentrations of cell-permeable metabolites for 48h.

Mean±SD (A,C) or mean+SD (F,I) are shown. Two-way ANOVA (A,C), two-way ANOVA with Holm-Sidak correction (F), one-way ANOVA with Holm-Sidak correction (I). Western blots are representative of two (B,G,J) or three (E) independent experiments. tRNA charging

analysis (D) was performed once for 100% Gln, and is representative of three independent experiments for 10% Gln. All other experiments were performed at least twice.

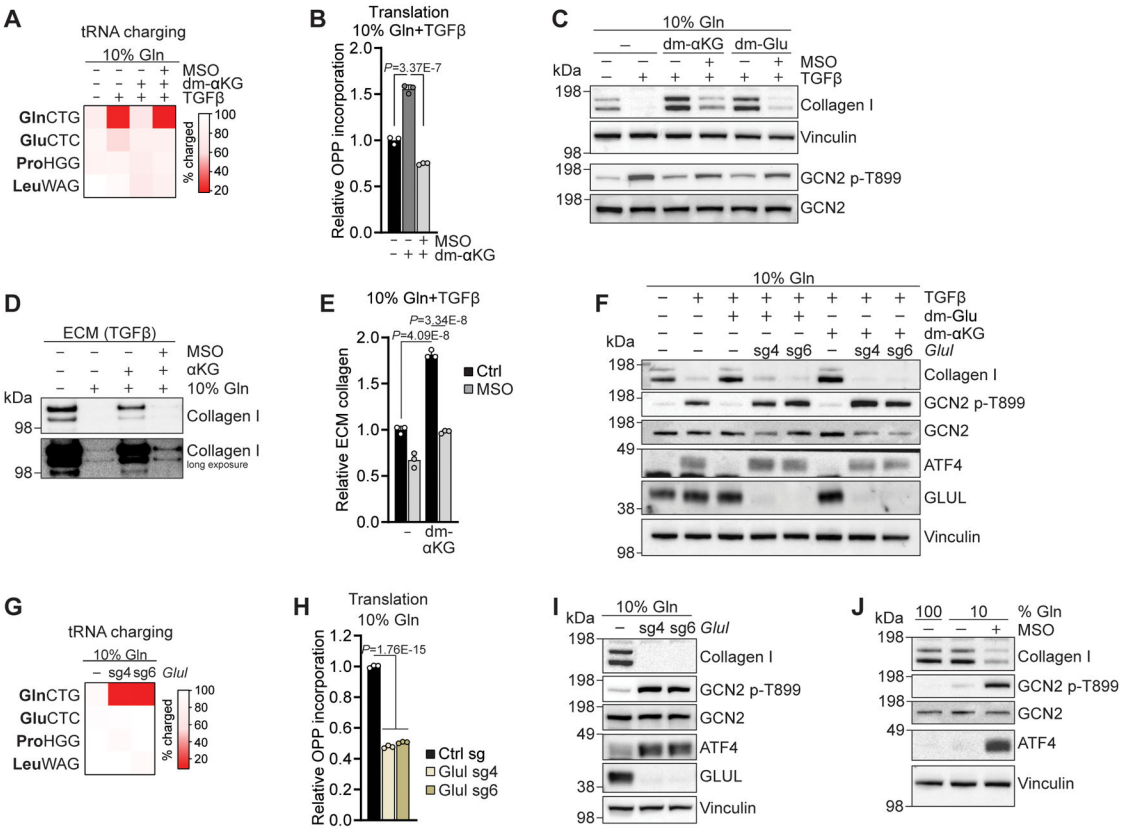

Figure 2: Glutamine *de novo* synthesis can maintain translation and collagen production when extracellular glutamine is limited.

(A) tRNA charging in NIH-3T3 cells cultured in 10% Gln and treated with TGFβ (2 ng/mL), dm-αKG (5 mM) and MSO (2 mM) for 48h. n=1 independent experiment. **(B)** Relative translation rate of NIH-3T3 cells cultured in 10% Gln and treated with TGFβ and dm-αKG and MSO. n=3 biologically independent samples. **(C)** Western Blot of NIH-3T3 cells cultured in 10% Gln and treated with TGFβ, dm-Glu (5 mM), dm-αKG and MSO for 48h. **(D)** Western Blot of ECM produced by confluent NIH-3T3 cells cultured in 100% or 10% Gln, treated with TGFβ and dm-αKG and MSO. **(E)** Collagen abundance in ECM produced by confluent NIH-3T3 cells cultured in 10% Gln, treated with TGFβ, dm-αKG and MSO. n=3 biologically independent samples. **(F)** Western Blot of NIH-3T3 cells expressing Ctrl or *Glul* sgRNA, cultured in 10% Gln and treated with TGFβ, dm-αKG or dm-Glu for 48h. **(G)** tRNA charging in NIH-3T3 cells expressing Ctrl or *Glul* sgRNA, cultured in 10% Gln for 48h. n=1 independent experiments. **(H)** Relative translation rate of NIH-3T3 cells expressing Ctrl or *Glul* sgRNA, cultured in 10% Gln for 48h. n=3 biologically independent samples. **(I)** Western Blot of NIH-3T3 cells expressing Ctrl or *Glul* sgRNA, cultured in 10% Gln for 48h. **(J)** Western Blot of NIH-3T3 cells cultured in 100% Gln or 10% Gln and treated with MSO for 48h.

Mean+SD (B,E,H) are shown. One-way ANOVA (H), one-way ANOVA with Holm-Sidak correction (B), two-way ANOVA with Holm-Sidak correction (E). tRNA charging analyses (A,G) are representative of two independent experiments. Western Blots (C,D,F,I,J) are

representative of two independent experiments. All other experiments were performed at least twice.

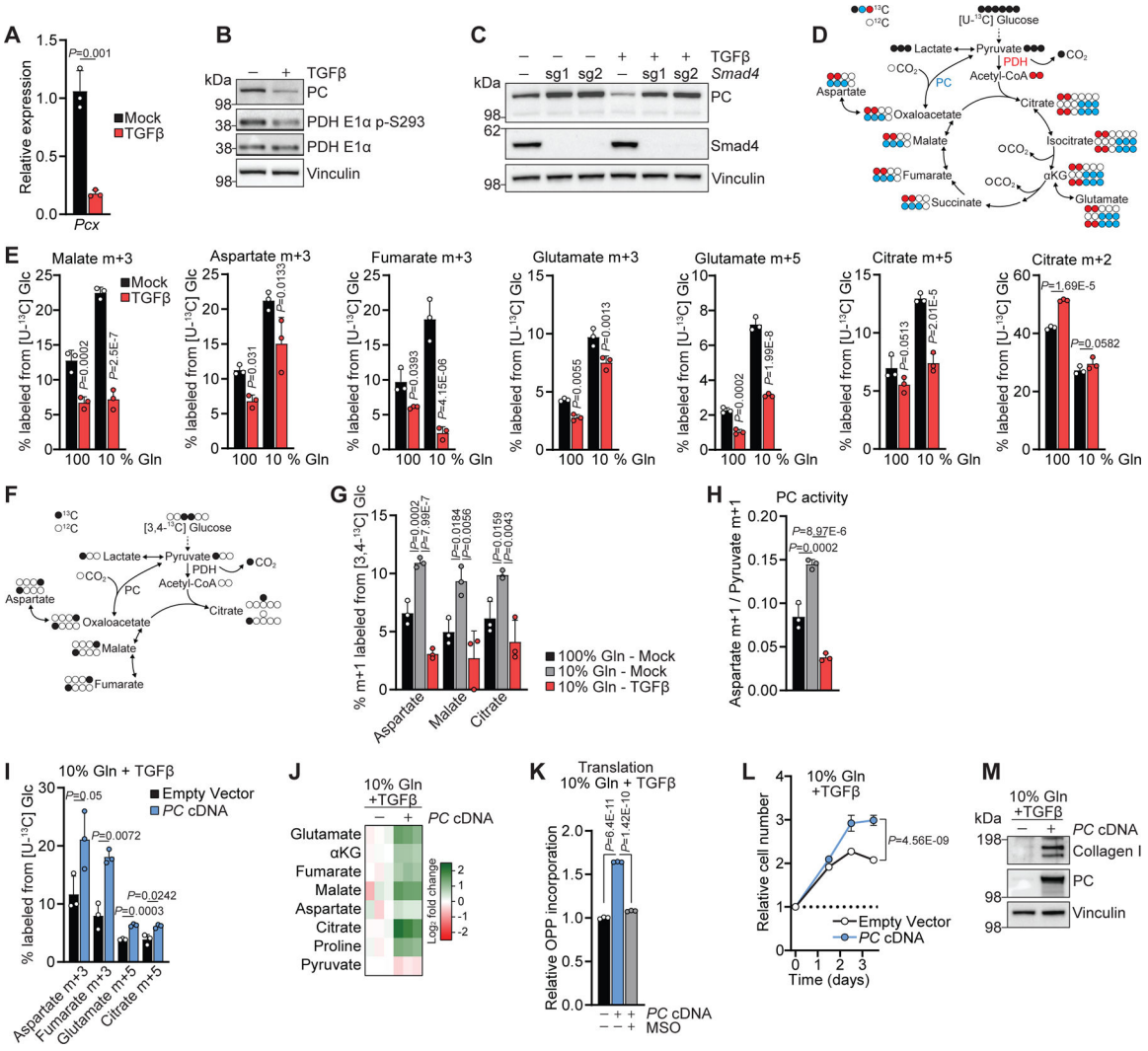

Figure 3: Pyruvate carboxylase suppression by TGFβ impairs TCA cycle anaplerosis, translation and collagen production in low glutamine.

(A) Pyruvate carboxylase (*Pcx*) mRNA expression in NIH-3T3 cells cultured in 100% Gln and treated with TGFβ for 24h. n=3 biologically independent samples. **(B)** Western Blot of NIH-3T3 cells cultured in 100% Gln and treated with TGFβ for 48h. **(C)** Western Blot of NIH-3T3 cells expressing Ctrl or *Smad4* sgRNA, cultured in 100% Gln and treated with TGFβ for 48h. **(D)** Schematic of [U-^{13}C]-glucose (Glc) tracing. **(E)** [U-^{13}C]-Glc tracing in NIH-3T3 cells cultured in 100% Gln or 10% Gln and treated with TGFβ for 48h. n=3 biologically independent samples. **(F)** Schematic of [3,4-^{13}C]-Glc tracing. **(G,H)** [3,4-^{13}C]-Glc tracing in NIH-3T3 cells cultured in 100% or 10% Gln and treated with TGFβ for 48h. M+1 labeling (G). PC activity (H). n=3 biologically independent samples. **(I)** [U-^{13}C]-Glc tracing in NIH-3T3 cells expressing empty vector or human *PC* cDNA cultured in 10% Gln in the presence of TGFβ for 48h. n=3 biologically independent samples. **(J)** Relative metabolite abundance in NIH-3T3 cells expressing empty vector or human *PC* cDNA, cultured in 10% Gln in the presence of TGFβ for 48h. n=3 biologically independent samples. **(K)** Relative translation rate of NIH-3T3 cells expressing empty vector or human

PC cDNA, cultured in 10% Gln in the presence of TGFβ and treated with MSO for 48h. *n*=3 biologically independent samples. **(L)** Growth curve of NIH-3T3 cells expressing empty vector or human *PC* cDNA, cultured in 10% Gln in the presence of TGFβ. *n*=3 biologically independent samples. Dashed line indicates cell number at d0. **(M)** Western Blot of NIH-3T3 cells expressing empty vector or human *PC* cDNA and cultured in 10% Gln in the presence of TGFβ for 48h.

Mean+SD (A,E,G-I,K) or mean±SD (L) are shown. Two-sided unpaired *t*-test (A), two-way ANOVA with Holm-Sidak correction (E), two-sided unpaired *t*-test with Holm-Sidak correction (I), one-way ANOVA with Holm-Sidak correction (G,H,K), two-way ANOVA (L). Western blots (B,C,M) are representative of two independent experiments. All other experiments were performed at least twice.

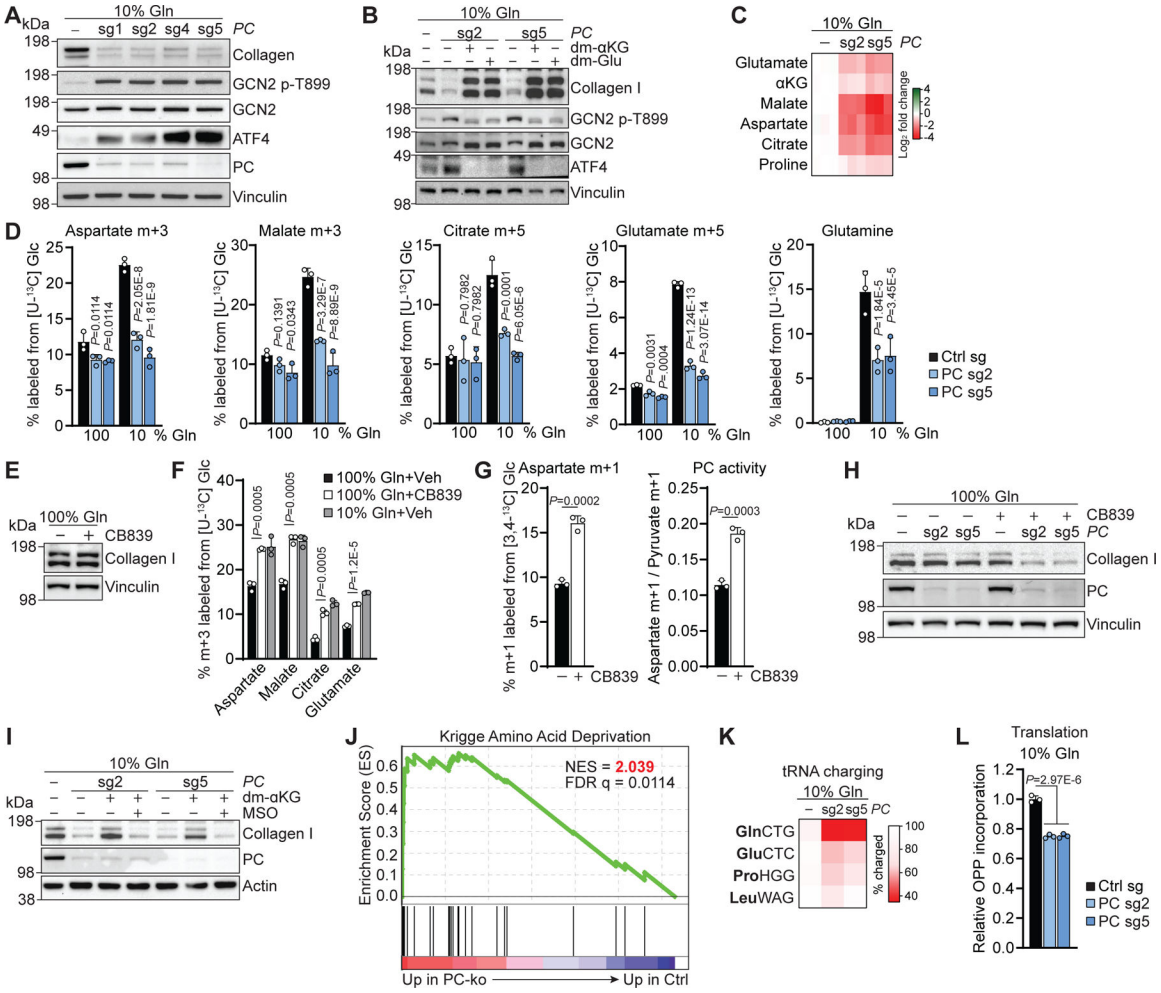

Figure 4: Pyruvate carboxylase anaplerosis is required for collagen production when extracellular glutamine levels are low.

(A,B) Western Blot of NIH-3T3 cells expressing Ctrl or *PC* sgRNA, cultured in 10% Gln for 48h (A) and treated with dm-αKG or dm-Glu for 48h (B). **(C)** Relative metabolite abundance in NIH-3T3 cells expressing Ctrl or *PC* sgRNA, cultured in 10% Gln for 48h. n=3 biologically independent samples. **(D)** [U-^{13}C]-Glc tracing in NIH-3T3 cells expressing Ctrl or *PC* sgRNA, cultured in 100% or 10% Gln for 48h. n=3 biologically independent samples. **(E)** Western Blot of NIH-3T3 cells cultured in 100% Gln and treated with CB839 (1 μM) for 48h. **(F)** [U-^{13}C]-Glc tracing in NIH-3T3 cells cultured in 100% or 10% Gln and treated with CB839 for 48h. n=3 biologically independent samples. **(G)** [3,4-^{13}C]-Glc tracing in NIH-3T3 cells cultured in 100% Gln and treated with CB839 for 48h. n=3 biologically independent samples. **(H)** Western Blot of NIH-3T3 cells expressing Ctrl or *PC* sgRNA, treated with CB839 for 48h. **(I)** Western Blot of NIH-3T3 cells expressing Ctrl or *PC* sgRNA, cultured in 10% Gln and treated with dm-αKG and MSO for 48h. **(J)** Gene set enrichment analysis (GSEA) of *PC*-ko compared to control NIH-3T3 cells cultured in 10% Gln. n=2 (Ctrl sg), n=4 (*PC*-ko) biologically independent samples. **(K)** tRNA charging in NIH-3T3 cells expressing Ctrl or *PC* sgRNA, cultured in 10% Gln for 48h. n=1 independent

experiment. **(L)** Relative translation rate of NIH-3T3 cells expressing Ctrl or *PC* sgRNA, cultured in 10% Gln for 48h. n=3 biologically independent samples.
Mean+SD (D,F,G,L) are shown. Two-way ANOVA with Holm-Sidak correction (D), one-way ANOVA with Holm-Sidak correction (F), two-sided unpaired *t*-test (G), one-way ANOVA (L). Western blots are representative of three (A) or two (B,E,H,I) independent experiments. tRNA charging analyses (K) are representative of two independent experiments. RNA-sequencing (J) was performed once. All other experiments were performed at least twice.

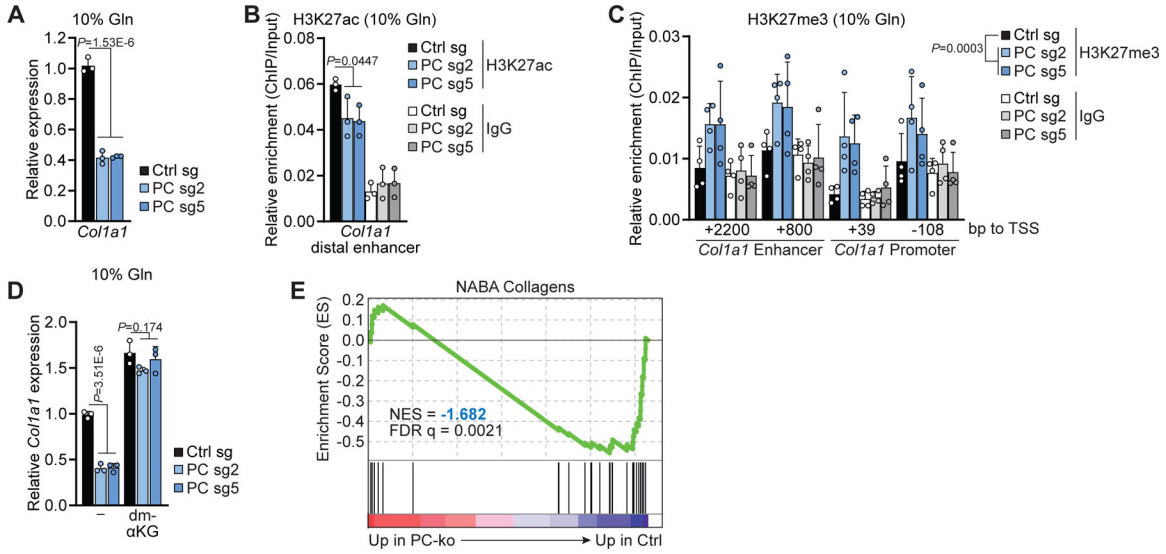

Figure 5: Pyruvate carboxylase anaplerosis supports collagen transcription when extracellular glutamine levels are low.

(A) *Col1a1* mRNA expression in NIH-3T3 cells expressing Ctrl or *PC* sgRNA, cultured in 10% Gln for 48h. n=3 biologically independent samples. **(B,C)** H3K27ac (B) or H3K27me3 enrichment (C) in NIH-3T3 cells expressing Ctrl or *PC* sgRNA, cultured in 10% Gln for 48h. n=3 (B), n=4 (C) independent experiments. TSS; transcriptional start site. **(D)** *Col1a1* mRNA expression in NIH-3T3 cells expressing Ctrl or *PC* sgRNA, cultured in 10% Gln for 48h and treated with dm-αKG. n=3 biologically independent samples. **(E)** GSEA in *PC*-ko compared to control NIH-3T3 cells. n=2 (Ctrl sg), n=4 (*PC*-ko) biologically independent samples.

Mean+SD (A-D) are shown. One-way ANOVA (A,B,D), two-way ANOVA (C) analyzing the effects of *PC*-ko on H3K27me3 across the indicated genomic regions. RNA-sequencing (E) was performed once. All other experiments were performed at least twice.

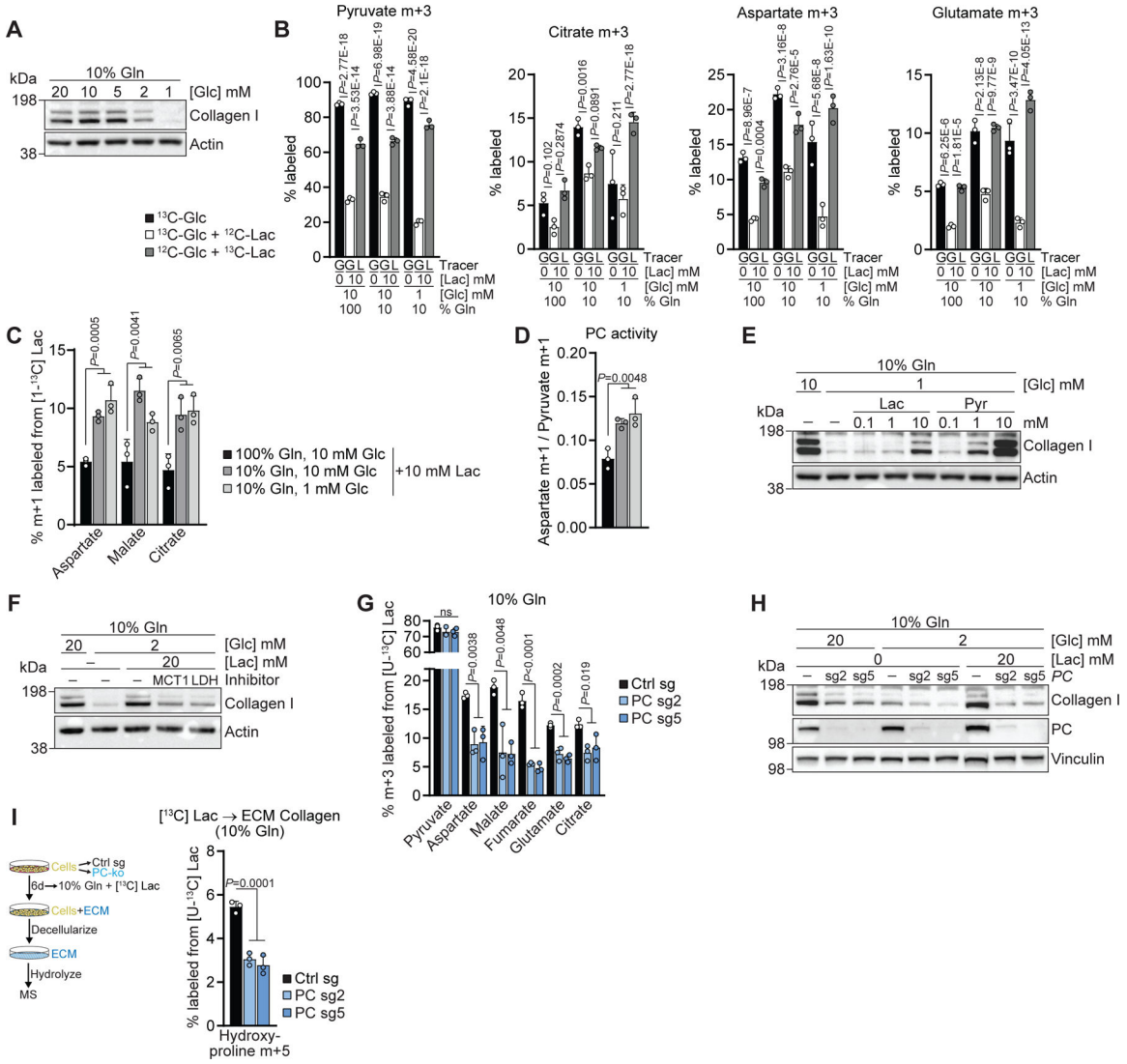

Figure 6: Lactate supports collagen production via pyruvate carboxylase when glucose and glutamine are limiting.

(A) Western Blot of NIH-3T3 cells cultured in 10% Gln and the indicated concentrations of D-glucose for 48h. **(B)** [U-^{13}C]-Glc and [U-^{13}C]-Lac tracing. NIH-3T3 cells were cultured for 48h in 100% or 10% Gln in the presence of 10 or 1 mM D-glucose alone or with 10 mM sodium lactate. n=3 biologically independent samples. **(C,D)** [1-^{13}C] Lac tracing in NIH-3T3 cells cultured for 48h in 100% or 10% Gln in the presence of 10 or 1 mM D-glucose and 10 mM sodium lactate. M+1 labeling (C). PC activity (D). n=3 biologically independent samples. **(E)** Western Blot of NIH-3T3 cells cultured in 10% Gln and 10 or 1 mM D-glucose and treated with sodium lactate or sodium pyruvate for 48h. **(F)** Western Blot of NIH-3T3 cells cultured in 10% Gln and 20 or 2 mM D-glucose for 72h and treated with AZD3965 (MCT1 inhibitor, 5 μM) or sodium oxamate (LDH inhibitor, 10 mM). Sodium lactate was added in the last 48h. **(G)** [U-^{13}C]-Lac tracing. NIH-3T3 cells expressing Ctrl or *PC* sgRNA were cultured in 10% Gln, 10 mM D-glucose and 10 mM sodium lactate for 48h. n=3 biologically independent samples. **(H)** Western Blot of NIH-3T3 cells expressing Ctrl or

PC sgRNA, cultured in 10% Gln and the indicated concentrations of D-glucose and sodium lactate for 48h. **(I)** [U-^{13}C]-Lac tracing into collagen secreted into the ECM. Confluent NIH-3T3 cells expressing Ctrl or *PC* sgRNA were cultured in 10% Gln supplemented with [U-^{13}C]-Lac for 6d. n=3 biologically independent samples.
Mean+SD (B-D,G,I) are shown. Two-way ANOVA with Holm-Sidak correction (B), one-way ANOVA (C,D,G,I). Western blots are representative of two (A,E) or three (F,H) independent experiments. All other experiments were performed at least twice.

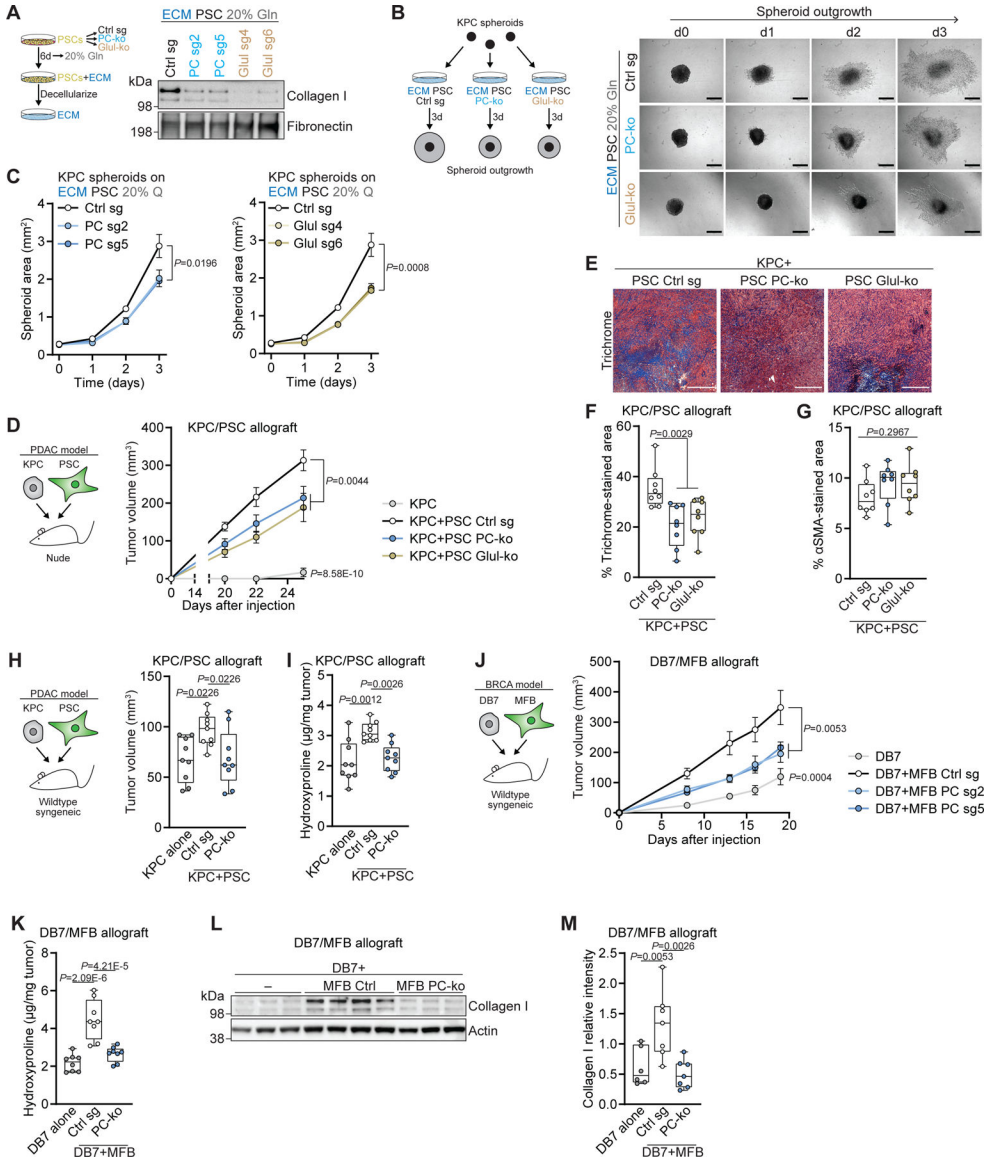

Figure 7: Fibroblast pyruvate carboxylase supports pancreatic and mammary tumor growth and fibrosis.

(A) Western Blot of ECM generated by confluent PSCs expressing Ctrl, *PC* or *Glul* sgRNA cultured in 20% Gln. **(B,C)** Outgrowth of KPC spheroids on ECM generated by confluent PSCs expressing Ctrl, *PC* or *Glul* sgRNA cultured in 20% Gln. Representative images (B) and quantification (C) are shown. Scale bar=500 μm. n=4 (Ctrl-sg, *PC*-sg2, *Glul*-sg6), n=3 (*PC*-sg5, *Glul*-sg4) biologically independent samples. **(D-G)** KPC cells were injected s.c. into nude mice, alone or with PSCs expressing Ctrl, *PC* or *Glul* sgRNA. **(D)** Growth curve of KPC/PSC allografts. n=8 biologically independent tumors. **(E)** Representative images of Masson's Trichrome staining of KPC/PSC allografts. Scale bar=500 μm. **(F,G)** Quantification of Masson's Trichrome (F) or αSMA staining (G) of KPC/PSC allografts. n=8 biologically independent tumors. **(H,I)** KPC cells were injected s.c. into syngeneic wildtype mice, alone or with PSCs expressing Ctrl or *PC* sgRNA. **(H)** Volume of KPC/PSC allografts 8 days after injection. n=9 biologically independent tumors. **(I)** Collagen levels in

KPC/PSC allografts 8 days after injection. *n*=9 biologically independent tumors. **(J-M)** DB7 cells were injected s.c. into wildtype syngeneic mice, alone or with MFBs expressing Ctrl or *PC* sgRNA. **(J)** Growth of DB7/MFB allografts. *n*=7 (d19 MFB *PC*-sg2), *n*=8 (all others) biologically independent tumors. **(K)** Collagen levels in DB7/MFB allografts 8 days after injection. *n*=8 biologically independent tumors. **(L)** Western Blot of DB7/MFB allografts 8 days after injection. **(M)** Collagen I band intensity relative to actin from (L) and Extended Data Fig. 6M. Samples derive from the same experiment and gels/blots were processed in parallel. *n*=6 (DB7), *n*=7 (DB7+MFB Ctrl, DB7+MFB PC-ko) biologically independent tumors.

Mean±SEM (C,D,J) or median with 25% to 75% percentile box and min/max whiskers (F-I,K,M) are shown. Two-way ANOVA (C,D,J) analyzing the effects of *PC*-ko or *Glul*-ko on spheroid or tumor growth over time, one-way ANOVA (F,G), one-way ANOVA with Holm-Sidak correction (H,I,K,M). Western blot (A) is representative of two independent experiments. Western blot (L) was performed once with 3–4 biologically independent tumors. Spheroid experiments were performed twice. Tumor growth, staining and hydroxyproline experiments were performed once with multiple biologically independent tumors.